AFRL-SR-AR-TR-04-

0613

REPORT DOCUMENTATION PAGE

Public reporting burden for this collection of information is estimated to average 1 hour per response, including the time for reviewing the data needed, and completing and reviewing this collection of information. Send comments regarding this burden estimate or any reducing this burden to Washington Headquarters Services, Directorate for Information Operations and Reports, 1215 Jefferson Davis Highway, Suite 1204, Arlington, VA 22202-4302, and to the Office of Management and Budget, Paperwork Reduction Project (0704-0188), Washington, DC 20503

1. AGENCY USE ONLY (Leave blank)	2. REPORT DATE	3. REPORT TYPE AND DATES COVERED
	11/30/04	Final Performance Report for the period 7/1/02-12/31/04

4. TITLE AND SUBTITLE
Advanced Polymer Composite Molding Through Intelligent Process Analysis and Control

5. FUNDING NUMBERS
F49620-02-1-0370

6. AUTHOR(S)
Bob Minaie and Alex Mamishev

7. PERFORMING ORGANIZATION NAME(S) AND ADDRESS(ES)

Mechanical Engineering Department
EGCB 212
University of South Alabama
Mobile, AL 36688

Electrical Engineering Department
Box 352500
University of Washington
Seattle, WA 98195

8. PERFORMING ORGANIZATION REPORT NUMBER

9. SPONSORING / MONITORING AGENCY NAME(S) AND ADDRESS(ES)

NL

10. SPONSORING / MONITORING AGENCY REPORT NUMBER

11. SUPPLEMENTARY NOTES

12a. DISTRIBUTION / AVAILABILITY STATEMENT
Approve for Public Release:Distribution Unlimited

12b. DISTRIBUTION CODE

13. ABSTRACT ***(Maximum 200 Words)***

In this project, process analysis of Resin Transfer Molding (RTM) was carried out and adaptive process control models were developed. In addition, a non-invasive sensor was manufactured to monitor the filling pattern and provide feedback during adaptive control.

Adaptive process control strategies based on several control models including linear model and recursive least square model were developed. Some of these models were implemented within a LabVIEW user interface. Simulation methodologies were also developed for comprehensive analysis of the RTM process.

A transparent and flexible sensor array was fabricated to non-invasively monitor the fill front location. To analyze the sensor signal, LabVIEW programs were written in modules that can be embedded into the data acquisition system. Another sensor array with multiple sensing elements was also designed to *simultaneously* monitor both the fill front location and the degree of cure. The multiplexing electronics needed for this multi-element sensor array was fabricated. The first generation of this sensor system was used to monitor the fill front location in molds of varying thickness and material.

This report presents the aforementioned work in three separate sections: (1) process analysis and adaptive control modeling, (2) manufacturing of non-invasive sensor, and (3) list of publications resulting from this project.

14. SUBJECT TERMS

15. NUMBER OF PAGES

16. PRICE CODE

17. SECURITY CLASSIFICATION OF REPORT	18. SECURITY CLASSIFICATION OF THIS PAGE	19. SECURITY CLASSIFICATION OF ABSTRACT	20. LIMITATION OF ABSTRACT
Unclassified	Unclassified	Unclassified	None

NSN 7540-01-280-5500

Standard Form 298 (Rev. 2-89)
Prescribed by ANSI Std. Z39-18
298-102

EXECUTIVE SUMMARY

Resin Transfer Molding (RTM) is a composite manufacturing process that produces high-strength and lightweight parts for aerospace, naval, automotive, and sports applications. During filling stage of RTM, there exists uncertainties such as the race tracking and resin viscosity changes due to the cure kinetics. As a result, the filling pattern becomes non-repeatable from part to part, and dry spot may form. To overcome the problem, flow control methods have to be used in RTM. In this project, various adaptive control strategies were developed to regulate the flow rate using implicit mold filling simulation. The objective of the control strategies is to simultaneously drive the flow front from different gates to the exit vent in order to eliminate or significantly reduce dry spot formation by controlling the flow rate at each gate. The flow progress along a spine line that links a gate to the vent is used for adaptive flow control. A finite element mesh with various vent locations and race tracking was numerically tested to evaluate the control strategies. The control strategy A, in which the flow rate is rearranged based on how far the flow front is from the vent, is the simplest and highly practical. The control strategy B is based on the Model Reference Adaptive System and it requires least adjustment during control. The Recursive Least Square method is applied in the control strategy C and D. The control strategy C is built with the assumption that the movement of flow front is determined by the unfilled area and flow rate. On the other hand, the combination of the simplified one-dimensional and two-dimensional flow model yields the control strategy D and has satisfactory control performance. Mold filling control test cases were numerically studied by adopting control strategies A and D. The results showed that control strategies A and D can effectively control the flow rates at the gates and successfully drive the flow front to the vent and, as a result, achieve a dry-spot-free mold filling.

The enabling technique for experimental adaptive control of the RTM process is non-invasive monitoring of the fill front position and degree of cure of the resin. Successful implementation of a sensing system capable of meeting these criteria can result in a high yield of composite parts. This study articulates the possibility of a hybrid sensing system for multi-parameter monitoring during RTM. It addresses fundamental engineering trade-offs between penetration depth and signal strength, discussing how to account for fringing electric field (FEF) effects present in the system. FEF effects may hinder the measurement accuracy of the sensor system. This report describes how these effects are addressed using a mapping algorithm that is developed using numerical simulations of the experimental setup. Modeling of the FEF effects helps to achieve high measurement accuracy of the fill front location.

This report presents the aforementioned work in three separate sections: (1) process analysis and adaptive control modeling, (2) manufacturing of non-invasive sensor, and (3) list of publications resulting from this project. Further details on this research can be found in the cited publications resulting from this project in section 3.

20041230 042

SECTION 1: PROCESS ANALYSIS AND ADAPTIVE CONTROL MODELING

INTRODUCTION

Resin Transfer Molding (RTM) is a manufacturing process used to produce polymer composite parts for aerospace, naval, automotive, and sports applications. This process has many advantages such as net-shape production, low injection pressure, and low cost tooling. However, RTM process can result in high scrap rate for the parts due to high level of process disturbances such as varying preform permeability distribution and uncertain resin cure kinetics. Reducing the scrap rate is important for advancing the current RTM manufacturing capability for the next generation mass production applications.

Mold filling simulation [1-6] is a promising tool to help engineers to reduce the scrap rate. Ideally, by using mold filling simulation, one can predict the Last Point to Fill (LPF) and then place the vent at LPF to reduce/prevent dry spot formation. Dry spot formation is a major reason to cause defective composite part and it happens if the LPF location does not coincide with the vent location and the entrapped air cannot be properly expelled. The mold filling simulation requires one to input the accurate material properties including preform permeability, fiber volume fraction, and resin viscosity to predict the filing pattern. However, in real RTM practice, it is often difficult to know accurate fiber preform permeability. As a result, the LPF location cannot be precisely predicted using the aforementioned numerical design tools. In addition, race-tracking effects [7] can significantly vary from one batch cycle to another batch cycle because of the operation uncertainty involved in cutting and fitting the fiber preform into the mold cavity. The uncertainties in preform permeability and race-tracking introduce substantial disturbances and uncertainties into the RTM process. Consequently, the LPF location usually does not remain in the same position during the RTM batch cycle production.

To eliminate the dry spot problem caused by flow disturbance and uncertainties during RTM process, flow control methods [11-22] have been used to drive the flow and yield dry-spot-free mold filling pattern. In recent years, various researchers have proposed model-based control strategies for RTM mold filling process [8-19]. Since the simulation time scale, which is taken to run the numerical simulation of RTM mold filling for control strategies, exceeds the control interval scale, Artificial Neural Network (ANN) strategy has been suggested [8] to substitute the numerical simulations. Feedback control strategy with features such as online parameter estimation or local optimal control has been proposed [9]. This control strategy needs a predetermined flow front pattern or injection conditions, which may be unknown or unsuitable due to some uncertainties. Researchers have also suggested the use of a number of inlets/vents in the RTM mold and subsequent opening or closing of these gates (switching control) to provide appropriate control actions during filling [10], and auxiliary gate was used to counteract a disturbance during filling [18]. This approach improves the controllability but some gates, such as sequential gates and auxiliary gates, are restricted to be secondary or sometimes are not used in certain control scenarios and hence may increase the equipment cost.

Due to the recent sensor technology development, process control systems are expected to have the capability to sense the filling front position in real time and feedback the filling front location to online process control. Sensing technologies such as SMARTweave [20], linear

sensor [21], on-chip dielectric sensor [22], and Fringe Electric Field array system [23] have been developed to measure the filling front location during the RTM process. Other measuring techniques such as laser ultrasonic sensing [24], fiber optic sensing [25], and video camera may be also available.

In this project, our goal is to develop adaptive control algorithms to achieve the control objective of reducing/eliminating the dry spot formation by regulating the LPF location in real time so that it coincides with the vent. The pressures/flow rates at the inlet gates are manipulated to drive the LPF location to coincide with the predetermined vent location; all gates are treated equally as injection gates. The filling pattern, in which all flow fronts move to the vent almost simultaneously along the spine line, is regarded as the optimum filling pattern. Therefore, one can achieve the optimum mold filling processing by running the simulation only once. The adaptive control algorithm is based on fixed gate and vent designation, no special gates and/or vents such as auxiliary gates or transferable gates are needed.

Initially an isothermal adaptive control system was developed to adjust the inlet pressure to achieve the control objective [26]. However, that approach was limited to inlet pressure adjustment and simple geometry mold filling. Then, an isothermal adaptive control system was developed to adjust flow rates to achieve control objective for complex geometries and it was validated on simulated flow control test problems. Four control strategies were tested for simple geometry. This section of the report presents the following: the principles and governing equations of numerical simulation for RTM mold filling are described next. Then, the details of the four proposed control strategies are described followed by presentation of sample results and conclusions.

RTM MODELING

In order to simulate the mold filling process of RTM, several assumptions need to be made to simplify the problem. In general, the preplaced fiber reinforcement in the mold cavity is assumed to be rigid during the molding process. There is no exchange of mass between the solid and the fluid. The solid and fluid have constant densities. Inertia effects are neglected because of the slow resin flow. Surface tension is considered negligible as compared with the dominant viscous force. Furthermore, there is no fluid ahead of the front and the preform is assumed fully saturated with the resin in the wetted region behind the front.

Flow Modeling

Darcy's law for flow through porous media is used to describe resin flow in fiber. The law can be written in the form:

$$\vec{v} = -\frac{\bar{\bar{k}}}{\mu} \cdot \nabla P \qquad (1)$$

where $\vec{v}$ is the velocity vector, ∇P is the pressure gradient, μ is the viscosity, and $\bar{\bar{k}}$ is the permeability tensor.

Control Volume Finite Element Method (CVFEM) is used for the RTM filling simulation. Based on the mass balance, a suitable approximation of the pressure gradient in the control volume centered at node i will result in a system of nonlinear equations [2]:

$$\Delta t \cdot a_i P_i = \Delta t \cdot a_{ij} P_{ij} + \varepsilon \cdot Vol \cdot \left(F^{old} - F\right) \tag{2}$$

where Δt is the time interval, P_{ij} is the pressure of j neighbor node around node i, a_{ij} is the coefficient, which is depended on permeability, viscosity, element properties, and control volume properties and can be derived from equation (1) by the integration of whole control volume boundary. F^{old} is the filling fraction of the control volume at the previous time step. $F = 1$ indicates that the node/control volume is completely filled, $F = 0$ means that the resin has not reached the control volume at all, and $0 < F < 1$ indicates that the node/control volume is partially filled.

There are two numerical methods to solve Eq. 2. One group of methods [1,2] uses an explicit method, whose time steps are subject to a Courant criterion. The alternative and more efficient approaches [5,6] are implicit, which are free of the Courant criterion, i.e., the time step could be set to any value.

In this project, an implicit method is employed to solve flow through preform [5]. The main advantages of implicit method are independent of time step and efficient for the simulation of the large and complex mesh. The next time step can be set to any required value, thus it is more suitable for our adaptive control studies.

ADAPTIVE CONTROL METHODOLOGIES

On-line flow control methods based on the flow rate or pressure control of multiple gates provide an effective mean of controlling the RTM filling pattern and has caught much attention in recent years [8-19]. Here, four control methods are presented and tested, all of the four methods are based on manipulation of flow rate, the inputs for control are the distances between flow front and vent along the shortest path from several control gates to the vent. Another isothermal adaptive control system was also developed to adjust the inlet pressure to achieve the control objective and details of that model are given in [26]

Spine Line Construction

Figure 1 shows the distance between flow front and vent for a simple geometry. Dijkstra's algorithm [29] is applied to find shortest path from a gate to the vent for complex geometry. The shortest path is a sequential node chain, whose length is shortest among all possible node chains from gate to vent. The algorithm is described in the following procedure (find all shortest paths from any node to the starting node s):

Dijkstra's Algorithm

Begin

$d_s = 0$, *s is the starting node*

$d_i = \infty$, *for* $i \neq s$

$E = \{all\ nodes\}$
$S = \{s\},\ T = E - S$
Loop until T is empty
find $v_m \in T$ *with minimum* d_m
from all linkage (v_m, v_s) *with* $v_s \in S$
$d_m = d_s + length((v_m, v_s))$
v_s *is stored as upstream node of* v_m
$S = S + v_m$
$T = T - v_m$
end loop
end

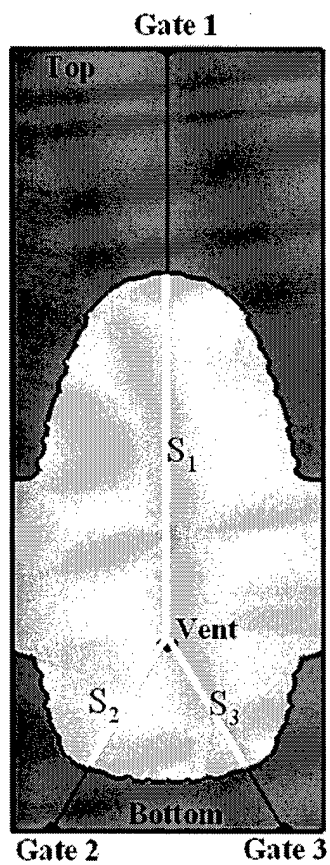

Figure 1. The Distances between Flow Front and Vent for Simple Geometry (Flat)

In the above procedure, pair (v_m, v_s) should be one edge of one element. After the procedure, any shortest path, which starts at the starting node in the procedure, can be tracked from the ending node via one upstream node by one upstream node. Therefore, if one vent and

multi-gate is arranged, Dijkstra's Algorithm can start at the vent, and then the shortest path can be tracked from gate.

Control Strategy A

As a rule of thumb, if the flow front moves to the vent almost simultaneously from all directions and the flow front in the final process stage ends very close to the vent, an ideal mold filling process and good part quality can be expected. Thus, it is intuitive to increase the flow rate of one gate when its flow front is behind the flow fronts controlled by other gates. With considering that flow rate is proportional to square of flow front distance to vent when resin is driven to vent circularly, the simplest way to adjust flow fronts is to set the flow rate proportionately by square of distance between flow front and vent. Based on Fig. 1, the flow rates of three gates are manipulated as follows:

$$Q_i = Q_{total} \cdot \frac{S_i^2}{S_1^2 + S_2^2 + S_3^2}, \quad i = 1, 2, 3 \tag{3}$$

where Q_i is flow rate of ith gate, Q_{total} is the total flow rate, and S_i is distance from flow front of ith gate to vent.

Control Strategy B

A Model Reference Adaptive System (MRAS) [30] is employed to construct the control algorithm for achieving the control objective. In this adaptive system, a reference model is specified and the process will follow the reference model's behavior. The reference model is chosen to be in the following form [26]:

$$\frac{dx_m}{dt} = \dot{x}_m = -a_m x_m + b_m u_c \tag{4}$$

where a_m and b_m are chosen constants which direct the model's performance to satisfy certain performance requirements. x_m is the controlling variable and u_c is the output variable. The control rule is chosen to be:

$$\frac{Q}{Q_{ref}} = a \cdot 1 + b \cdot x = a + b \cdot \frac{S^2}{S_{init}^2} \tag{5}$$

where Q is flow rate, Q_{ref} is initial flow rate/referred flow rate, and S is the distance between flow front and vent, S_{init} is the initial distance between flow front and vent, i.e. the distance from gate to vent along the spine line.

Based on Lyapunov stability theory [30-31], the adaptation rule can be derived as following:

$$\frac{da}{dt} = -\gamma_1 \cdot e \tag{6.a}$$

$$\frac{db}{dt} = -\gamma_2 \cdot e \tag{6.b}$$

where $e = x - x_m$, x_m is the desired/reference x value. In this study, the uniform movement of flow front to vent is accepted as the reference model.

The adaptive rule always decreases the error. For example, if $e > 0$, i.e., the flow front is more advanced than desired, the a and b will decrease, then the controlled flow rate will decrease and the flow front will slow down in order to meet the desired flow front.

Control Strategy C

When there is input/signal noise, digital filter and parameters estimation algorithm are needed for the control method. The Recursive Least Square Methods (RLS) are the adaptive estimation algorithms that have built-in filtering mechanisms [31]. The control strategy C is based on RLS algorithm. Since the movement of flow front is mainly related with the unfilled area and flow rate, the following equation is constructed for the control strategy C:

$$\frac{\dot{S}S}{\dot{S}_m S_{init}} = a \cdot \frac{S^2}{S_{init}^2} + b \cdot \frac{Q}{Q_{ref}} \tag{7}$$

where $\dot{S}_m$ is the flow front velocity of the desired filling pattern, a and b are the dynamically estimated parameters which can be evaluated by using the RLS algorithm expressed as follows:

$$k(n) = \frac{\lambda^{-1} P(n-1) u(n)}{1 + \lambda^{-1} u^T(n) P(n-1) u(n)} \tag{8.a}$$

$$y(n) = w^T(n-1) u(n) \tag{8.b}$$

$$e(n) = d(n) - y(n) \tag{8.c}$$

$$w(n) = w(n-1) + k(n) e(n) \tag{8.d}$$

$$p(n) = \lambda^{-1} p(n-1) - \lambda^{-1} k(n) u^T(n) p(n-1) \tag{8.e}$$

where $w(n)$ is the estimated vector, λ is the forgetting factor, $u(n)$ is the input variables, $d(n)$ is the desired output, $y(n)$ is the estimated output, $e(n)$ is error, $P(n)$ is a symmetric gain matrix, n is number of time steps.

For the control strategy C, $y = \frac{S\dot{S}}{\dot{S}_m S_{init}}$, $u_1 = \frac{S^2}{S_{init}^2}$, $u_2 = \frac{Q}{Q_{ref}}$, $w_1 = a$, $w_2 = b$. After a and b are estimated, the flow rate Q is calculated by Eq.7 with the theoretical $S\dot{S}$ and S^2, and is adjusted by the error as follows:

$$Q = Q_{ref}\left(\frac{\frac{S\dot{S}}{\dot{S}_m S_{init}} - a\cdot\frac{S^2}{S_{init}^2}}{b} + k_e \cdot e\right) \tag{9}$$

where k_e is the adjusting factor, e is the previous error of flow front distance.

Control Strategy D

With consideration of one-dimensional flow and two-dimensional flow (see Figure 2), the following system equation is established for adaptive control:

$$\frac{Q}{Q_{ref}} = a\cdot\frac{\dot{S}}{\dot{S}_m} + b\cdot\frac{\dot{S}S}{\dot{S}_m S_{init}} \tag{10}$$

where a and b are the dynamically estimated parameters.

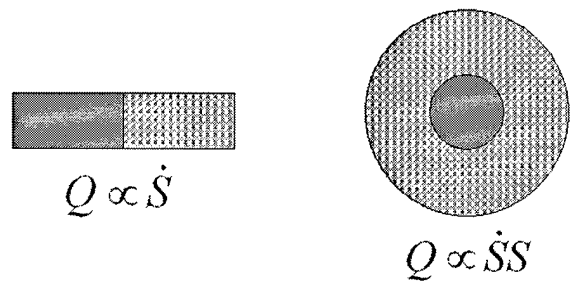

Figure 2. 1D and 2D Simplification for Control Strategy D

For the control strategy D, $y = \frac{Q}{Q_{ref}}$, $u_1 = \frac{S}{S_{init}}$, $u_2 = \frac{S\dot{S}}{\dot{S}_m S_{init}}$, $w_1 = a$, and $w_2 = b$ are variables in RLS. After a and b are estimated using Eq. 8, the flow rate Q is calculated by Eq. 10 with the theoretical S and $S\dot{S}$, and is adjusted by the error of flow front distance as follows:

$$Q = Q_{ref}\left(a\cdot\frac{\dot{S}}{\dot{S}_m} + b\cdot\frac{\dot{S}S}{\dot{S}_m S_{init}} + k_e \cdot e\right) \tag{11}$$

RESULTS AND DISCUSSION

In order to test and compare the four control algorithms, a simple geometry with various permeability distribution and vent locations was used to conduct flow control simulations. After the comparison, two complex geometries were used for validation of control strategy A and D.

The dimension of the simple geometry is 0.2m*0.08m*0.01m (Length*Width*Thickness); the finite element mesh has 1667 nodes and 3200 triangular elements. The permeability is 8.7e-12m^2 and the porosity is 0.55. Three gates are fixed at two ends (see Figure 1). One vent locates at central line, and four vent cases are 0.050m, 0.100m, 0.144m, and 0.172m from bottom. Vent-050, Vent-100, Vent-144, and Vent-172 are used to represent these vent cases in the following discussion. There are 2 cases for permeability distribution, i.e., uniform and race-tracking at all edges.

All cases of vent locations and race-tracking were studied for all control strategies and without any control. The predetermined flow rate setting of without control is based on control strategy A in the initial situation, i.e., the predetermined flow rate of gate is proportional to the square of distance between gate and vent. The desired filling time is 49.16s, and the desired filling pattern is that the resin is driven from gate to vent uniformly and arrives the vent simultaneously.

Each control strategy may require some constants/parameters to be setup before use. There is no any constant or parameter to be setup for control strategy A. $\gamma_1 = 2.5$ and $\gamma_2 = 1.0$ for control strategy B. The forgetting factor of control strategy C and D is 1.0, and the initial symmetric gain matrix $p(0) = 0.1I$ for control strategy C and $p(0) = 10.0I$ for control strategy D, where I is unit matrix. The k_e =20 and 10 for control strategy C and D respectively.

Dry Spot

The objective of adaptive control is to eliminate/reduce dry spot. In the present study, it is achieved by mean of driving flow fronts from different gates to arrive the vent simultaneously. The results are listed in Table 1. The unfilled area is regarded as dry spot area when all neighbor nodes of vent are filled. All of the four control strategies are successful in eliminating dry spot or reducing dry spot, the average of dry spot area drops from about 1.8% without control to no dry spot for race-tracking at all edges, and drops from about 11% to 1.6% for uniform permeability. The detail filling patterns of one case (Race-tracking, Vent-144) are benchmarked in Figure 3. According to Figure 3, although the resin arrives the vent before the part is filled completely, the air is always able to get out through vent since the vent is not completely entrapped by the resin. However, if vent is too close to gate, dry-spot-free may be unachievable for some cases, for example, Vent-144 and Vent-172 with uniform permeability (see Figure 6 for Vent-144).

Table 1. Comparison of Dry Spot Results

Void (%Total Porous Volume), Permeability: Race-tracking

Ctrl Strategy	Vent				Summary	
	050	100	144	172	Average	Worst
NONE	0.00	4.43	2.70	0.00	1.78	4.43
A	0.00	0.00	0.00	0.00	0.00	0.00
B	0.00	0.00	0.00	0.00	0.00	0.00
C	0.00	0.00	0.00	0.00	0.00	0.00
D	0.00	0.00	0.00	0.00	0.00	0.00

Void (%Total Porous Volume), Permeability: Uniform

Ctrl Strategy	Vent				Summary	
	050	100	144	172	Average	Worst
NONE	0.03	19.16	17.20	7.22	10.90	19.16
A	0.00	0.07	1.75	4.59	1.60	4.59
B	0.06	0.00	1.36	4.30	1.43	4.30
C	0.00	0.00	1.38	6.28	1.91	6.28
D	0.00	0.00	1.24	4.27	1.37	4.27

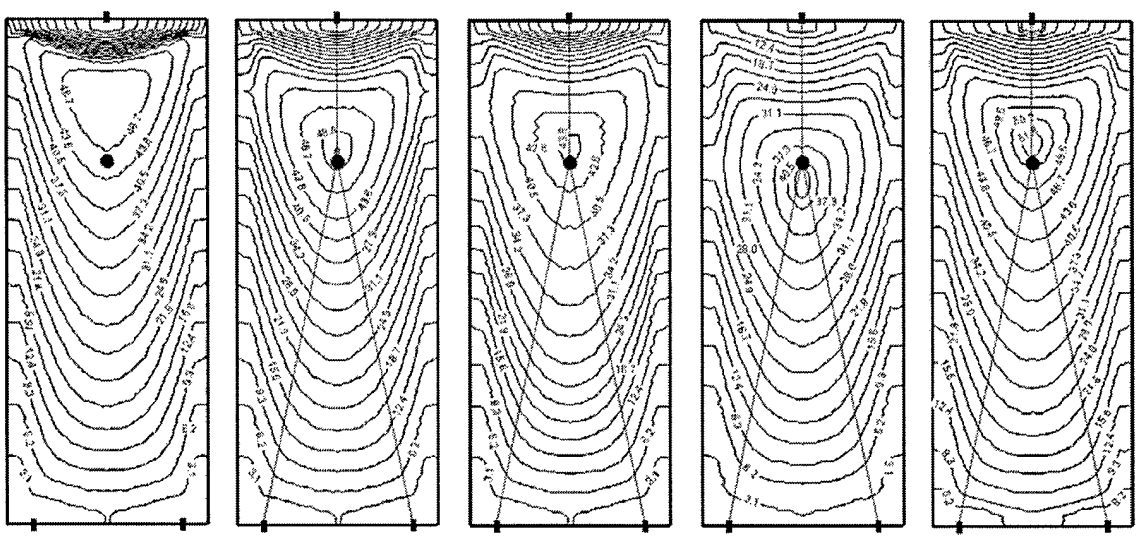

Without Control Control Strategy A Control Strategy B Control Strategy C Control Strategy D

Figure 3. Filling Patterns for Race-tracking, Vent-144 Case

LPF Location

One of the RTM process design considerations for full impregnation is to place a vent at the location where the Last Point to Fill (LPF) will occur. This design ensures the air being properly expelled, reduces the air entrapment, and prevents the dry spot formation. Therefore, the distance between LPF and vent is a reasonable performance index that specifies the quality of filling pattern.

Table 2 shows the result of LPF for all cases. The LPF is improved by control strategies from about average 7.0 percent to about 1.6 percent for race-tracking at all edges. Although resin

from all gates arrive at vent almost simultaneously, dry spots are formed for most of cases with uniform permeability and corresponding LPFs are far from vent. These dry spots are due to the fact that flow front from one gate does not converge to vent at the end of filling (see Figure 4 for illustration), thus the injection adjustment for one gate loses its flow front controllability. However, dry spot areas are reduced significantly for uniform permeability because that resins from three gates are driven to vent simultaneously along the shortest path.

Table 2. Comparison of LPF Results

LPF Location (% Maximum Span), Permeability: Race-tracking

Ctrl Strategy	Vent				Summary	
	050	100	144	172	Average	Worst
NONE	1.86*	13.00	11.14	1.86	6.96	13.00
A	1.86	1.86	1.86	0.00	1.40	1.86
B	1.86	0.00	1.86	0.00	0.93	1.86
C	1.86	1.86	1.86	1.86	1.86	1.86
D	1.86	1.86	1.86	0.00	1.40	1.86

LPF Location (% Maximum Span), Permeability: Uniform

Ctrl Strategy	Vent				Summary	
	050	100	144	172	Average	Worst
NONE	1.86	13.98	31.95	19.05	16.71	31.95
A	1.49*	3.60	17.63	22.67	11.35	22.67
B	1.86	18.57	18.02	22.67	15.28	22.67
C	0.00	18.57	17.63	22.67	14.72	22.67
D	1.49	2.97	18.02	22.67	11.29	22.67

*: Due to mesh size, 1.86% and 1.49% mean that those LPFs are neighbor nodes of vent

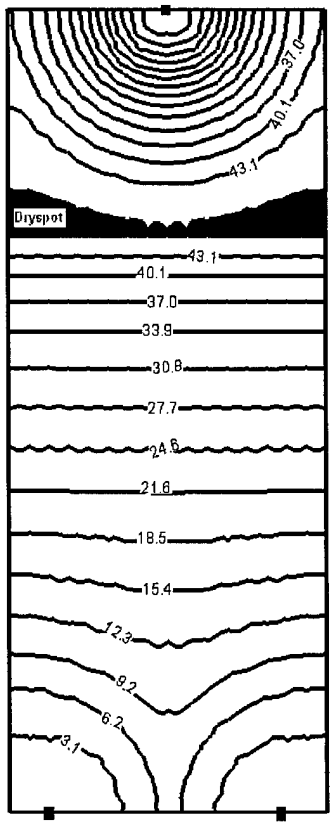

Figure 4. Filling Patterns (Control Strategy A) for Uniform, Vent-144 Case

Average Adjustment

In this study, the adaptive control is to manipulate the flow rate to achieve dry-spot-free. The amount of the flow rate adjusted is related to the practicability of the adaptive control system. Table 3 gives the result of average adjustment of flow rate for four control strategies. The control strategy A and B adjust the flow rate very smoothly. The manipulated variable of control strategy C is sharply adjusted. Although the average adjustment of control strategy C is about 5 percent of total flow rate, there are many steps for the flow rate to be adjusted more than 50 percent in control strategy C, the phenomena is illustrated in Figure 5. Both Table 3 and Figure 5 show that it is moderate for control strategy D to adjust the flow rate.

Table 3. Average Adjustment of Control System for all Cases

Average Adjust (%Total Flow Rate)				
Ctrl Strtg	Gate1	Gate2	Gate3	Average
A	1.10	1.10	2.19	1.46
B	1.74	1.74	2.56	2.01
C	4.89	4.89	5.59	5.12
D	1.70	1.70	2.14	1.85

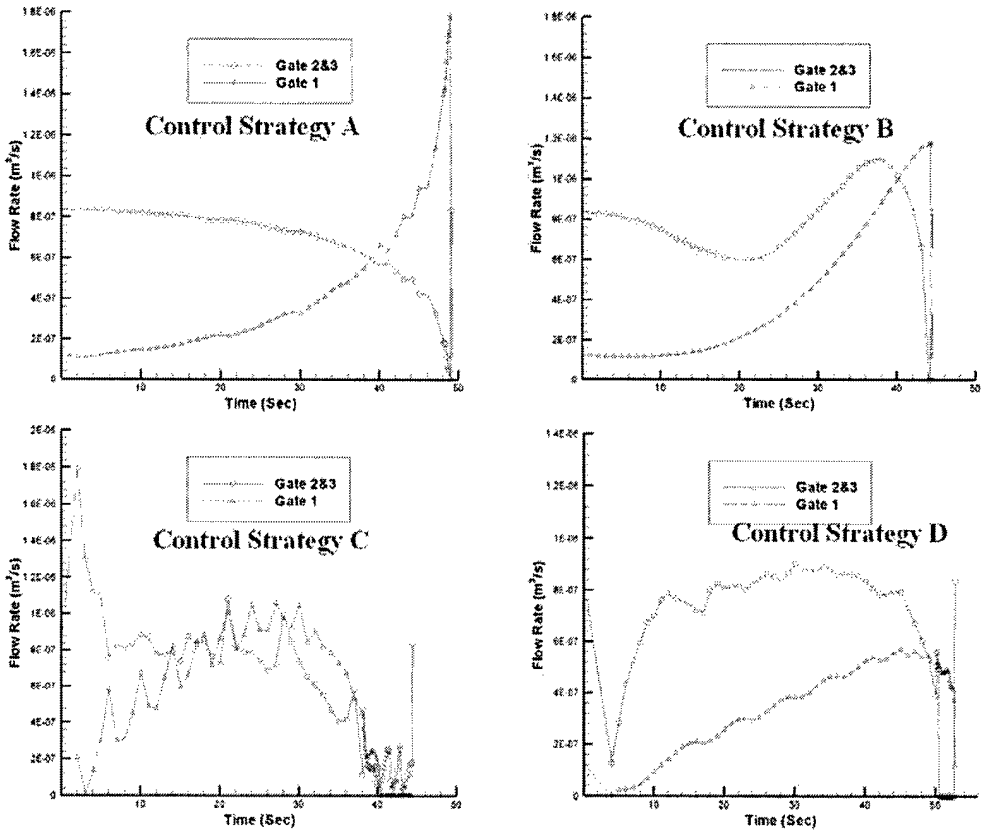

Figure 5. Flow Rate of All-Enhance, Vent-144 Case

Flow Front

The desired filling models of control B, C, and D are designed to achieve the uniform movement of flow front from all of gates to vent. Figure 6 shows the typical flow front movement from gates to vent. The result illustrates that all of the four control strategies work very well for the objective of driving flow fronts from gates to the vent simultaneously. The control strategy C drives the resin to the vent by almost constant movement. The control strategy A and D move the resin to the vent near the end of filling also by almost constant speed.

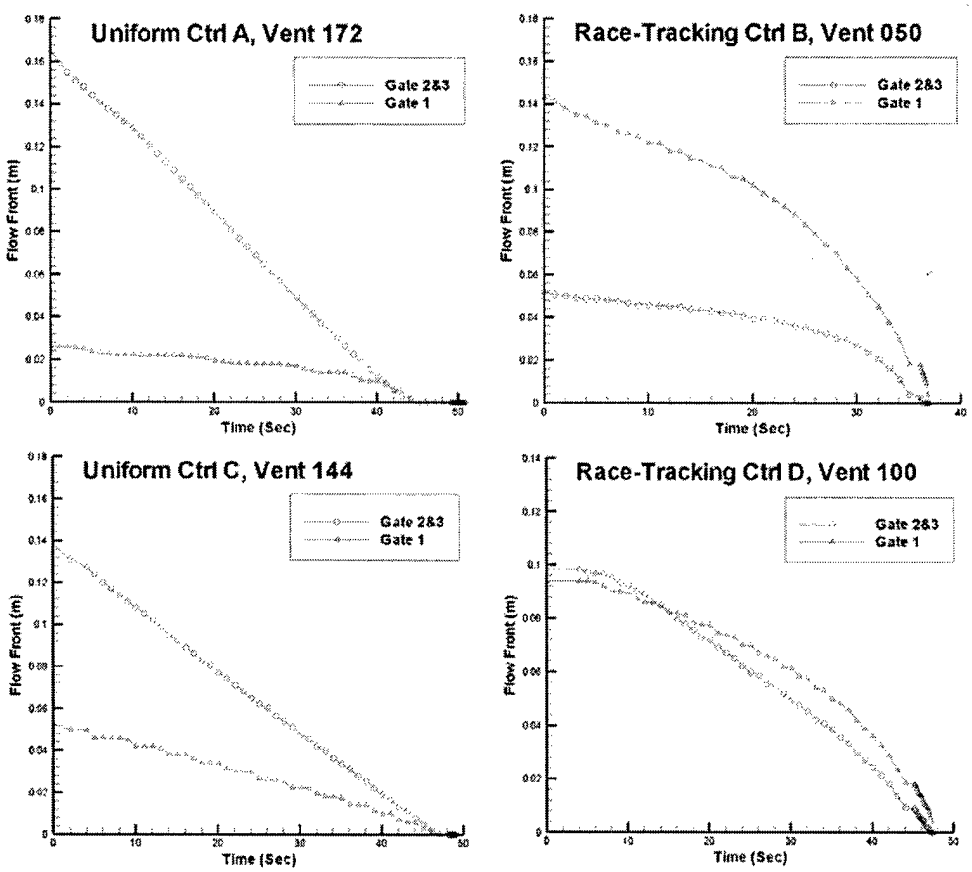

Figure 6. How Flow Front Moves to the Vent

CONCLUSIONS

In this study, adaptive control strategies to manipulate the flow rate were investigated for Resin Transfer Molding by isothermal numerical simulation. The objective of the control strategies is to drive the flow front to the vent simultaneously in order to eliminate/reduce dry spot. All of the adaptive control strategies worked very well to eliminate or reduce dry spot for different disturbances. The control strategy A, in which the flow rate is calculated based on how far the flow front is from the vent along the shortest path from the gate to the vent, is the simplest and highly practical. The control strategy B, which is constructed by the Model Reference Adaptive System, has the lowest average adjustment during control. The Recursive Least Square method is applied in the control strategy C and D. The system equation of control strategy C are generated with the assumption that the movement of flow front is determined by the unfilled area and flow rate, and the combination of the simplified one dimensional and two dimensional flow models yields the control strategy D. It was verified from simulated test cases that control strategies A and D consistently worked very well.

Further details on this research can be found in the cited publications resulting from this project in section 3 of this report.

REFERENCES

1. Bruschke, M.V. and S.G. Advani, "A Finite Element/Control Volume Approach to Mold Filling in Anisotropic Porous Media," *Polymer Composites*, Vol. 11, pp. 398-405, 1990.
2. Young, W.B., K. Han, L.H., Fong, L.J. Lee, "Flow Simulation in Molds with Preplaced Fiber Mats," *Polymer Composites*, Vol. 12, pp. 391-403, 1991.
3. Hournag, L. and C. Chang, "Numerical Simulation of Resin Transfer Molding in Molds with Preplaced Fiber Mats," *Journal of Reinforced Plastics and Composites*, Vol. 12, pp. 1081-1095, 1993.
4. Trochu F., R. Gauvin, D.M. Gao, "Numerical Analysis of the Resin Transfer Molding Process by the Finite Element Method," Advances in Polymer Technology, Vol. 12, No.4, pp. 21-26, 1993.
5. Voller, V. and S. Peng, "An Algorithm for Analysis of Polymer Filling of Molds," *Polymer Engineering and Science*, Vol. 35, pp. 1758-1765, 1995.
6. Chen, Y., K. Stelson and V. Voller, "Prediction of Filling Time and Vent Locations for Resin Transfer Molds," *Journal of Composite Materials*, Vol. 31, pp. 1141-1161, 1997.
7. Gokce A. and S.G. Advani, "Combinatorial Search to Optimize Vent Locations in the Presence of Disturbances in Liquid Composite Molding Processes," *Materials and Manufacturing Processes*, Vol. 18, No. 2, pp. 261-285, 2003.
8. Demirci, H.H. and J.P. Coulter, "Control Flow Progression during Molding Processes" *Journal of Materials Processing and Manufacturing Science*, Vol. 3, pp. 409-425, 1995
9. Berker, B. and J.Q. Sun, "Adaptive Control and On-line Permeability Estimation of Resin Transfer Molding for Composite Materials," *Journal of Materials Processing and Manufacturing Science*, Vol. 6(3), pp. 193-203, 1998.
10. Berker, B., P. Barooah, and J.Q. Sun, "Sequential Logic Control of Liquid Injection Molding with Automatic Vents and Vent-to-Gate Converters," *Journal of Materials Processing & Manufacturing Science*, Vol. 6, pp. 81-103, 1997.
11. Parthasarathy, S., S.C. Mantell, K.A. Stelson, S. Bickerton, and S.G. Advani, "Real-time Sensing and Control or Resin Flow in Liquid Injection Molding Processes," *Proceedings of the 1998 American Control Conference*, Vol. 4, pp. 2181-2184, 1998.
12. Berg, J. and V. Voller, "An Identification and Control Strategy for a Liquid Composite Molding Process," *Applied Mathematical Modeling*, Vol. 22, pp. 207-218, 1998.
13. Kang M.K., J.J. Jung, W.I. Lee, "Analysis of Resin Transfer Moulding Process with Controlled Multiple Gates Resin Injection," *Composite Part A: Applied Science and Manufacturing*, Vol. 31, pp. 407-422, 2000.
14. Nielsen, D. and R. Pitchumani, "Intelligent Model-Based Control of Preform Permeation in Liquid Composite Molding Processes with Online Optimization", *Composite Part A: Applied Science and Manufacturing*, Vol. 32, pp. 1789-1803, 2001.
15. Bickerton, S., H.C. Stadtfeld, K.V. Steiner, S.G. Advani, "Design and Application of Actively Controlled Injection Schemes for Resin Transfer Molding," *Composites Science and Technology*, Vol. 61, pp. 1625-1637, 2001.
16. Dunkers, J.P., K.M. Flynn, R.S. Parnas, D.D. Sourlas, "Model-Assisted Feedback Control for Liquid Composite Molding," *Composite Part A: Applied Science and Manufacturing*, Vol. 33, pp. 841-854, 2002.

17. Nielsen, D.R. and R. Pitchumani, "Closed-Loop Flow Control in Resin Transfer Molding Using Real-Time Numerical Process Simulations," *Composites Science and Technology*, Vol. 62, pp. 283-298, 2002.
18. Lawrence, J.M. et al., "An Approach to Couple Mold Design and On-line Control to Manufacture Complex Composite Parts by Resin Transfer Molding," *Composite Part A: Applied Science and Manufacturing*, Vol. 33, pp. 981-990, 2002.
19. Hsiao, K.T., M. Devillard, S.G. Advani, "Streamline Intelligent RTM Processing: From Design to Automation," *Proceeding of SAMPE 2003*, Long Beach, CA, May 2003.
20. Coulter, J.P., E.E. Hiuerey, J.M. Troiano, H.H. Demirci, and T.L. Nixon, "Real Time Sensing of Resin Flow Dynamics During Intelligent Molding," *Journal of Materials Processing and manufacturing Science*, Vol. 4, pp. 173-181, 1997.
21. Barooah, P., B. Berker, and J.Q. Sun, "Lineal Sensors for Liquid Injection Molding of Advanced Composite Materials," *Journal of Materials Processing & Manufacturing Science*, Vol. 6, pp. 169-183, Jan. 1998.
22. Day, D.R. et al. "New Dielectric Sensor for Statistical Process Control of Thermoset Molding," *Proceeding of the 49th Annual Technical Conference ANTEC*, Vol. 37, pp. 946-948, Montreal, Quebec, Canada, 1991.
23. Mamishev, A.V., Y. Du, B.C. Lesieutre, and M. Zahn, "Development and Application of Fringing Electric Field Dielectrometry Sensors and Parameter Estimation Algorithm," *Journal of Electrostatics*, Vol. 46, pp. 109-123, 1999.
24. Auaddison, R.C., Jr. et al., "In-site Process Monitoring Using Laser-Based Ultrasound," *IEEE Ultrasonics Symposium*, New York, NY, Vol. 2, pp. 1306, 1992.
25. Bernstein, J.R. and J.W. Wagner, "Fiber Optic Sensors for Use in Monitoring Flow Front in Vacuum Resin Transfer Molding Process," *Review of Scientific Instrument*, Vol. 68, pp. 5, May 1997.
26. Minaie B. and Y.F. Chen, "Adaptive Control of Filling Pattern in Resin Transfer Molding Process," *Journal of Composite Materials* (accepted).
27. Hsiao K.T., H. Laudorn, S.G. Advani, "Experimental Investigation of Heat Dispersion Due to Impregnation of Viscous Fluids in Heated Fibrous Porous Media During Composites Processing," *Transactions of ASME*, Vol. 123, pp. 178-187, 2001.
28. Advani, S.G., *Flow and Rheology in Polymer Composites Manufacturing*, The Netherlands: Elsevier Science B. V., 1994.
29. Dijkstra, E., "A note on two problems in connexion with graphs," *Numerische Mathematik*, 1, 269-271, 1959.
30. Astrom, K.J. and B. Wittenmark, *Adaptive Control*, Addison-Wesley, 1989.
31. Ogata, K., *Modern Control Engineering*, Prentice Hall, 1997.

SECTION 2: MANUFACUTURING OF NON-INVASIVE SENSOR

INTRODUCTION

Fill-front position has been identified as a crucial parameter in dry spot formation [1-5]. Previous attempts to regulate fill-front location have shown limited controllability [6-8].

Many techniques have been used to monitor the resin transfer molding process, including fiber optical sensing [9-11], ultrasound sensing [12,13], fluorescence [14], calorimetry [15], and DC resistance measurements [5,16-18] These techniques are similar in that they all require either embedded sensing elements or partial contact with the parts. DC resistance measurement arrays, such as SMARTWEAVE, provide the ability to monitor fill-front position and degree of cure simultaneously. However, this technique relies on point sensing, where the resolution of important parameters, like fill-front location, is limited by the number of sensor pixels the system can handle. A system capable of continuously sensing fill-front progression can more accurately determine the velocity and position of the fill-front.

A promising candidate technology to base an adaptive control system on is AC dielectrometry. This technique is capable of sensing fill-front location, curing, temperature, and viscosity simultaneously [19,20]. FDEMS is a commercially available AC dielectrometry system that relies on point sensing and requires direct contact and embedded parts [21-24]. It has been shown in [25,26] that AC dielectric sensors are capable of accurately measuring fill-front position and degree of cure. In [26], a linear dependence of the admittance signal on the fill-front position is shown. This particular type of sensor relies on fringing electric fields and allows continuous sensing of fill-front progression in one dimension. The system designed by Rooney et al. [25] is a three-channel sensing system capable of converting capacitance to voltage and correlating this to flow-front position. This system is limited to sensing fill-front location, and does not provide the ability to measure resin properties. The system discussed in this report is designed to perform spectroscopy measurements (i.e., measurements at multiple frequencies) and combine point sensing with continuous sensing.

Dielectric spectroscopy of material properties was deeply investigated by Von Hippel in the 1940's [27]. More advanced techniques based on the measurement of dielectric properties of polymer composites, including interdigital dielectrometry, were developed by Matis in the 1960's [28]. Microdielectrometry as a means of measuring dielectric properties in polymers was developed and used by Senturia's group in the early 1980's [29-31], and subsequently by other groups during the last ten years [32-35]. The recent trend has been to integrate dielectric spectroscopy into a self-contained system capable of measuring multiple parameters of interest for material manufacturing processes.

In the case of this study, viscosity, temperature, and degree of cure must be inferred from the measurements of capacitance and conductance between the sensor array electrodes. This project is focused on the design and implementation of a sensor system that can measure the desired parameters of interest with the required accuracy, spatial resolution, and speed. In order to measure viscosity, temperature, and degree of cure in 3D, a sensor that can perform spectroscopy measurements at many different points along the mold needs to be designed. Although spectroscopy measurements are inherently discrete in space and time, a large number of pixel elements will make these measurements more useful. Conversely, measurement of the

fill front does not require spectroscopy and should be sensed continuously for the most accurate results. Thus, a sensing system capable of measuring multiple parameters of interest should have multiple sensing elements. The first type of element should be designed to measure the fill-front location of a liquid material as it flows through the mold. The second type of element should be designed to perform dielectric spectroscopy measurements at discrete points in space. Both types of elements can be duplicated several times to compose a larger array of pixels. Figure 1 shows a conceptual illustration of how the flow front and spectroscopy pixels can be integrated into a hybrid sensor array. Figure 1 is designed to give the reader an idea of the global view that this report is driving towards, and is not meant to illustrate an existing sensing system.

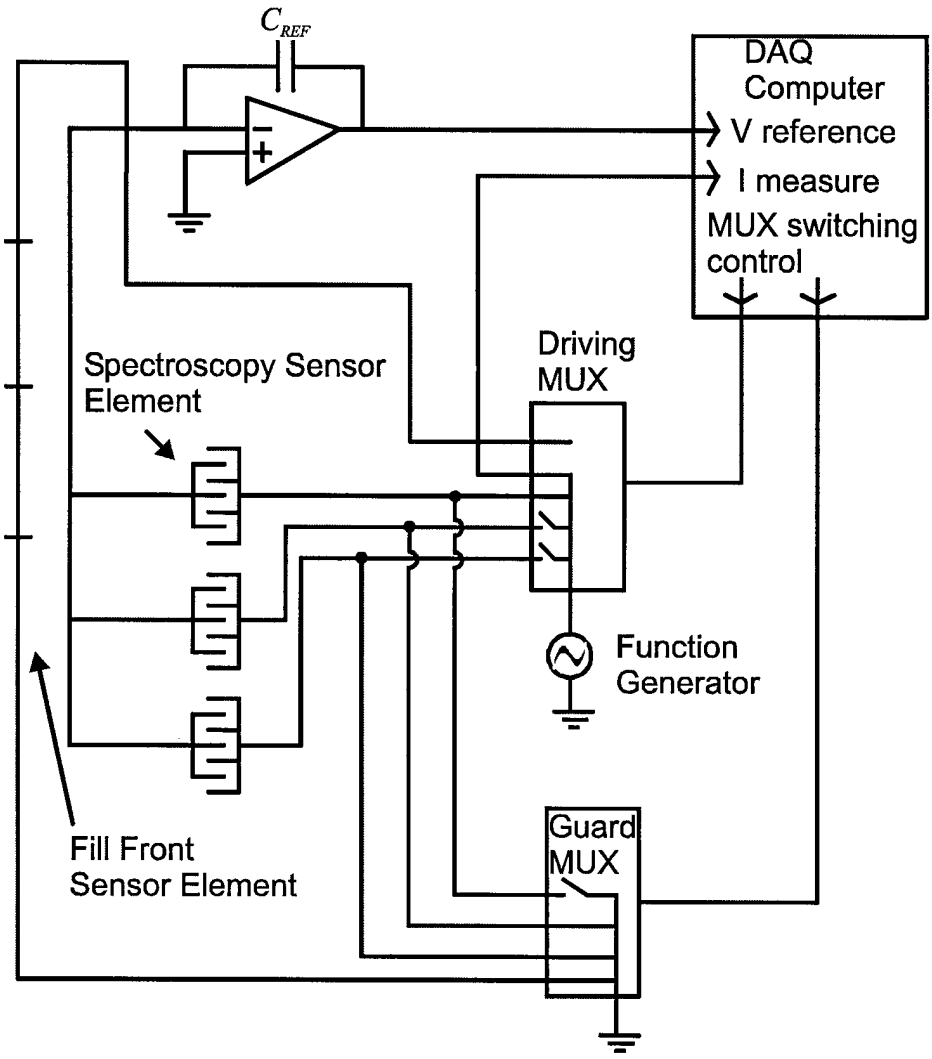

Figure 1. Conceptual layout of a hybrid sensor that shows fill front and spectroscopy sensing elements connected to multiplexing circuitry.

This report describes the design and testing of the fill front element of a multi-pixel sensor system. This is an important first step in the realization of a hybrid sensing system that

can be used for adaptive control in RTM. The design and testing of the spectroscopy sensor elements shown in Figure 1 will be detailed in a later publication. This sensor system will have continuous dielectric sensing capabilities for remote and in-situ monitoring of fill front position, viscosity, temperature, and degree of cure during resin transfer molding. These sensors will rely on continuous and simultaneous measurements of transadmittance matrix entries over a wide range of frequencies. The prototype sensor system described in this report has been integrated with a resin transfer molding apparatus, and is composed of three sensors, a three-channel circuit capable of measuring gain and phase, a function generator, DC power supply, and data acquisition software. An AC sinusoidal signal is supplied by the function generator to the bottom plate of the mold (aluminum). Electric field is generated between the bottom plate and the sensors resting on top of the upper polycarbonate (Lexan) plate of the mold. The sensors react to the changes in capacitance and conductance due to resin injection and progression through the mold. Numerical simulations of the sensors allow for calculation of fill-front position along the mold based on the measured signal strength.

The following section discusses the experimental system. The next section after that details experimental results obtained with several types of FEF sensors. Finally, conclusions are presented.

EXPERIMENTAL SYSTEM

An RTM laboratory setup, including the mold, resin flow system, and digital camera for flow verification, was used to simulate the industrial resin transfer molding process. To monitor important processing parameters, a sensor system with three channels and continuous sensing capability was designed and integrated into the resin transfer molding setup. A three-channel buffer circuit was custom-built for this project to interface with the sensor system and output the measurements in real-time using LabView software. This section discusses the elements of the RTM laboratory setup. Mold and materials are discussed, followed by the discussion of the sensor design and fabrication. Finally, the data acquisition circuit and software are presented.

RTM Laboratory Setup

Figure 2 shows the experimental system consisting of a resin transfer mold, a fluid delivery system, and sensors. The mold is rectangular with a transparent upper plate for visualization of the fill front. The working fluid is delivered to the mold using a pressurized reservoir. A video camera is mounted above the mold in a steel frame. Dielectric sensors are used to monitor the fill front. The pre-form used in this study is an open-celled polyurethane foam (MA70) with a uniform permeability throughout the material. The permeability of the medium is determined from Darcy's law using measured fill front velocities and pressure gradients. The foam has a solid fraction of 3.8%. The fill front velocity is calculated using change in fill front position over a known interval of time. The pressure gradient is obtained from pressure measurements within the mold cavity using a Wilkerson USG pressure gauge with a scale of 0 – 30 Hg. A mixture of 80% glycerin and 20% water is used as the working fluid. The viscosity of glycerin solution is similar to resins used and it also does not wick into the foam. This allows for easy cleaning and fast sequencing of the experiments. For filling experiments, the

dielectric properties of the working fluid need not be similar to that of industrial resins so long as the viscosities are similar and the fluids flow in the same manner. A rectangular aluminum mold 350 mm x 250 mm x 10 mm with one inlet port and one outlet port is used as the mold cavity. A 38 mm thick Lexan plate serves as the upper assembly of the mold. A digital video camera is mounted 1 m from the top of the mold to record independently the fill-front position. The mold is assembled by clamping the two aluminum plates together with bolts. Glycerin-water solution is delivered to the mold from the pressure pot using flexible tubing. The pre-form used is 19 mm shorter than the mold cavity to allow for pressure equalization on the leading edge to ensure a one-dimensional fill front. Multiple trials were performed to ensure repeatability of the system. Experiments were conducted for varying reservoir pressures ranging from 69 kPa (10 psi) to 114 kPa (16.5 psi), at room temperature.

Figure 3 shows the geometrical distribution of sensors on the top of the Lexan plate. This geometry allows for comprehensive and continuous sensing of the fill-front. The sensors are aligned parallel to the expected direction of the glycerin flow front movement. BNC cabling is used to connect the function generator to the top plate of the aluminum mold. For all experiments reported here, the function generator supplied a constant 6 V sinusoidal signal at 1 kHz driving frequency. An electric field is generated between the sensors and the mold with the applied signal. Progression of the fill-front is detected by continuously sensing a change in the complex gain, the ratio of the output and input voltages for each sensor pixel. Changes in capacitance and conductance are then inferred from changes in complex gain using a simple impedance divider circuit. Figure 4 shows the general schematic of the experimental system.

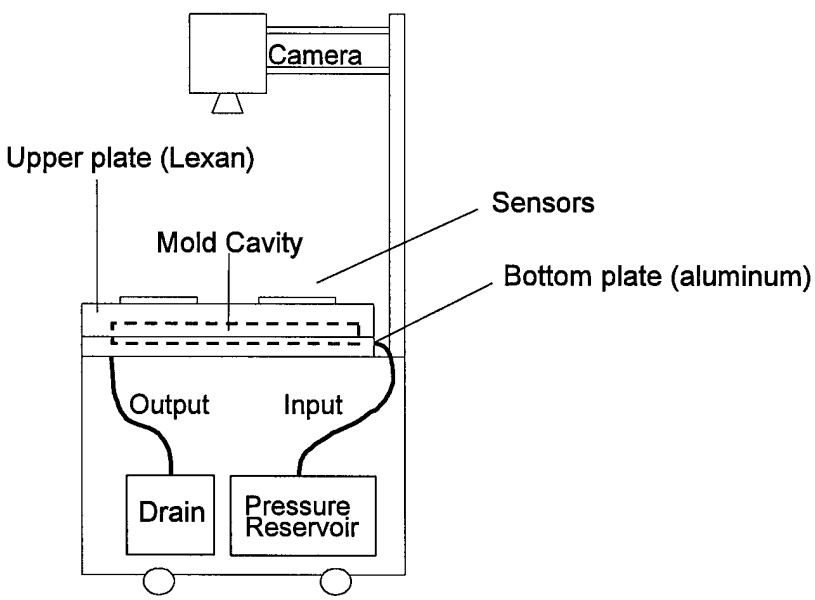

Figure 2. RTM mold and video camera that allows for independent measurements of fill-front position.

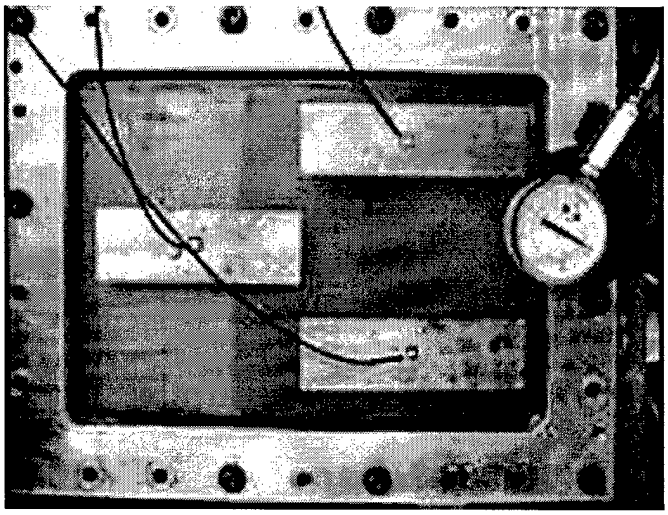

Figure 3. Experimental setup with distributed dielectric sensors.

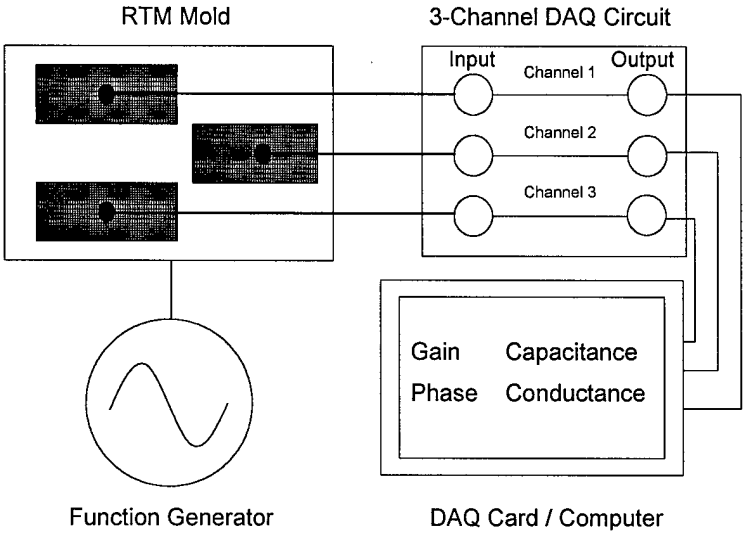

Figure 4. General schematic of the experimental system with data acquisition.

Sensors

Theory

It is well known that impedance cells can be used to sense the properties of dielectric materials [36,37]. In the simplest case, two parallel electrodes with equal but opposite surface charge densities σ_s have a potential difference

$$V = \phi_1 - \phi_2 \tag{1}$$

where ϕ_1 and ϕ_2 represent electric potential on each electrode. Since the potential difference is equal to the work required to move charge from one plate to the other,

$$V = \mathbf{E}d \tag{2}$$

where d is the distance between the electrodes. From Gauss' law, the electric field $\mathbf{E}$ between the electrodes is

$$\mathbf{E} = \frac{\sigma_s}{\varepsilon} \tag{3}$$

It follows that

$$V = \frac{\sigma_s}{\varepsilon} d = \frac{d}{\varepsilon A} Q \tag{4}$$

The total charge, Q, on both electrodes is proportional to the potential difference between the electrodes. The constant of proportionality is the capacitance and is given by

$$C = \frac{\varepsilon A}{d} \tag{5}$$

and the conductance is given by

$$G = \frac{\sigma A}{d} \tag{6}$$

where σ is the conductivity of the material.

When a dielectric material is passed between the plates of the mold, the capacitance C and conductance G change. Guard electrodes are usually included in the parallel-plate configuration to ensure a uniform electric field within the sensing area. Figure 5 shows the distribution of the electric field lines in a guarded parallel plate sensor. The figure shows that electric field lines are attracted to regions of greater permittivity, and thus how fringing fields

can exist even in guarded parallel plate sensors. A video camera is used to make independent measurements of the fill front position to test the accuracy of the sensor system. For the experiments reported here, a three-element dielectric sensor array is used to detect the fill-front position of glycerin-water solution as it is injected into a mold.

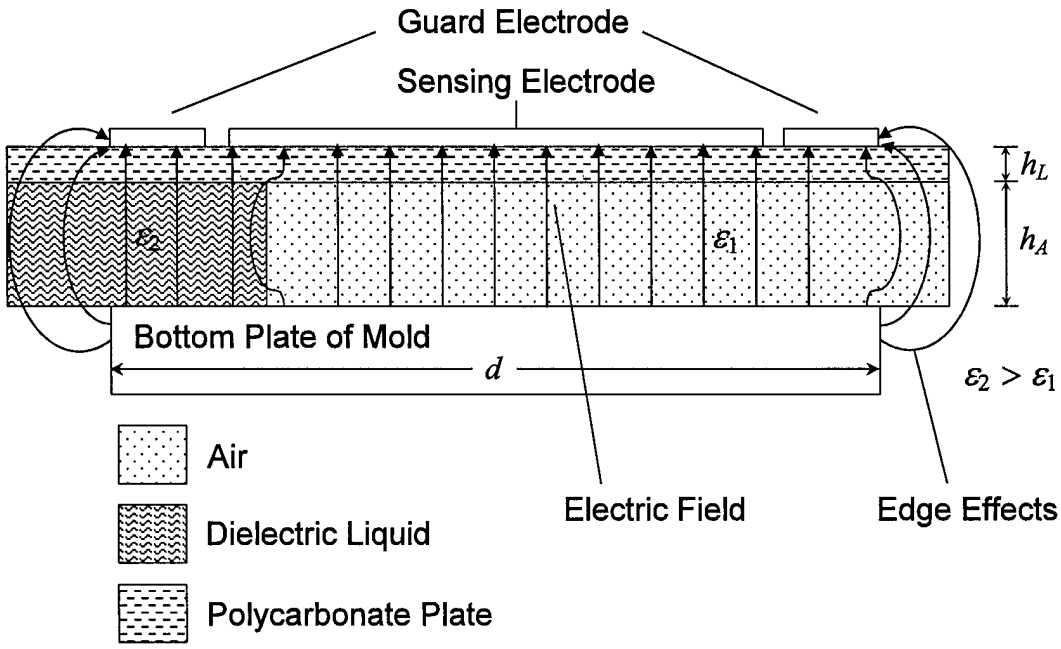

Figure 5. Distribution of electric field of the sensor including edge effects. Fluid flows into the mold cavity and position is inferred from changes in capacitance.

A 6 V amplitude sinusoidal input signal is applied to the bottom plate of the mold. Each sensor outputs to a channel on an impedance divider circuit. The complex voltage signal is fed into a PC via a DAQ card operating at 96 ks/s. Data acquisition software was written in LabView to convert the measured gain and phase to capacitance and conductance and display these values in real time.

Design Constraints

Figure 5 shows how the composition of the material can affect the uniformity of the electric field in the parallel-plate sensor. Besides material composition, the uniformity of the electric field is strongly dependent on the geometry of the sensor. For a parallel-plate configuration, the parameters of the setup that affect the uniformity of the electric field are the distance between the electrodes, the composition of the material, and the degree to which the electrodes are parallel. If the material between the electrodes is non-homogeneous or the distance between the electrodes varies considerably over the sensing area, the electric field can be non-uniform and the capacitance measured is then based on an average value of the dielectric permittivity over the sensing area. As long as the electrodes are parallel, the material homogeneous, and the distance between the electrodes is relatively small, the electric field will be uniform.

It may be possible to quantify the effect of the electric field for a given part geometry. A more practical solution, however, would be to utilize a fringing electric field (FEF) setup where the electric field fringes into the part and only one-sided access is needed. This would allow for point sensing within the part and allow for complex part geometries where parallel-plate setups become impractical.

The shape of the sensor can be designed to accommodate different mold geometries and for optimal adaptive control needs. Sensing area is the most important design criterion for parallel-plate sensors, and therefore long strips are commonly used. For FEF sensors, the spacing between electrodes determines the penetration depth. Longer and thinner sensor geometries will not accommodate as many electrodes as a wider design. For our purposes, however, one fringing electric field is adequate and therefore a longer and thinner sensor is realizable.

As demonstrated in [38], FEF sensors can be bent (e.g., wrapped around objects with complex geometries) with no measurable effect on their performance. This is of importance in composite material manufacturing processes where the mold geometry is complex. In addition, it may be possible to line the walls of the mold with complex sensor shapes in order to achieve more uniform sensing of the part. Parallel plate sensors can be designed to be thin, transparent, and flexible. The sensors can be laminated with a protective coating to ensure mechanical integrity under extreme temperatures and to prevent damage from spills.

Fabrication

Transparent dielectric sensor heads were fabricated using standard photolithography techniques: indium tin oxide (ITO) was evenly sputtered onto one side of a thin polyester film, a mask of the sensor electrode pattern was placed over the film, and exposed to UV light. The sensor pattern was etched into the ITO using bleach as an etching agent. Optically transparent glue was then used to attach an un-etched sheet of ITO film to the backside of the newly etched sheet. This blank sheet of ITO serves as the backplane for the sensor head. Finally, both sides of the sensor head were cold-laminated using commercially available lamination sheets, which serve as a protective coating against scratches. Coaxial cables are attached to the sensor head via zero-insertion-force (ZIF) connectors. The transparency of the sensor head allows for complete visual confirmation of flow front position and offers the possibility of enhancing the system with an infrared sensor. Figure 6 shows the complete ITO sensor head.

Figure 6. Flexible, transparent sensor head.

Data Acquisition and Sensor Interface

The data acquisition and sensor interface consists of a custom-designed buffer circuit that interfaces the sensor head with a computer, and software that displays sensor measurements in real-time. For every operating frequency, when a dielectric material is placed between two parallel conducting electrodes, the resultant circuit can be modeled as an RC parallel combination. For sensor impedance measurements, the custom designed three-channel circuit utilizes a floating-voltage measurement technique. Figure 7 shows a single measurement channel, where the voltage divider is formed by the sensor and the reference impedance. The voltage is sensed by an ultra-high input impedance op-amp in a voltage follower configuration. The reference impedance value is set close to the value of the expected measurement impedance. When the material under test is only weakly conductive, the lumped circuit approximation can be simplified to a single capacitor. The reference capacitance value used in these experiments is 7 pF for each of the three channels.

The coaxial cable connecting a sensor to the measurement circuit is 1.5 m long. To eliminate the effect of capacitance between the inner and outer conductor in the cable, the output of the voltage follower is fed back to the cable's shielding conductor. The technique ensures that there is no potential difference between the inner conductor carrying the sense signal and the shielding conductor around it. The shield potential is also used to keep the guard electrode at the same potential as the sensing electrode.

For the specified sensor geometry, the capacitances in the voltage divider are usually very small. The leakage current from the op-amp input causes static charge to accumulate on the sensor electrodes, as well as on the reference capacitor. To discharge both capacitances, a reed relay is connected between the middle of the voltage divider and ground terminal. The switch is automatically closed for a short period of time before each measurement.

The outputs of the three-channel circuit and the function generator signal are connected to a NI-DAQ 6035E data acquisition card operating at 96 kS/s. The card simultaneously samples all four voltage signals. In addition, it provides the digital signal for controlling the discharge relays. It should be noted that the input impedance of the NI card when connected to the output of the op-amp can greatly decrease the phase margin of the circuit, causing high-frequency instability. To prevent possible oscillatory behavior, a 1 kΩ resistance can be added between each of the circuit's outputs and the positive power supply rail.

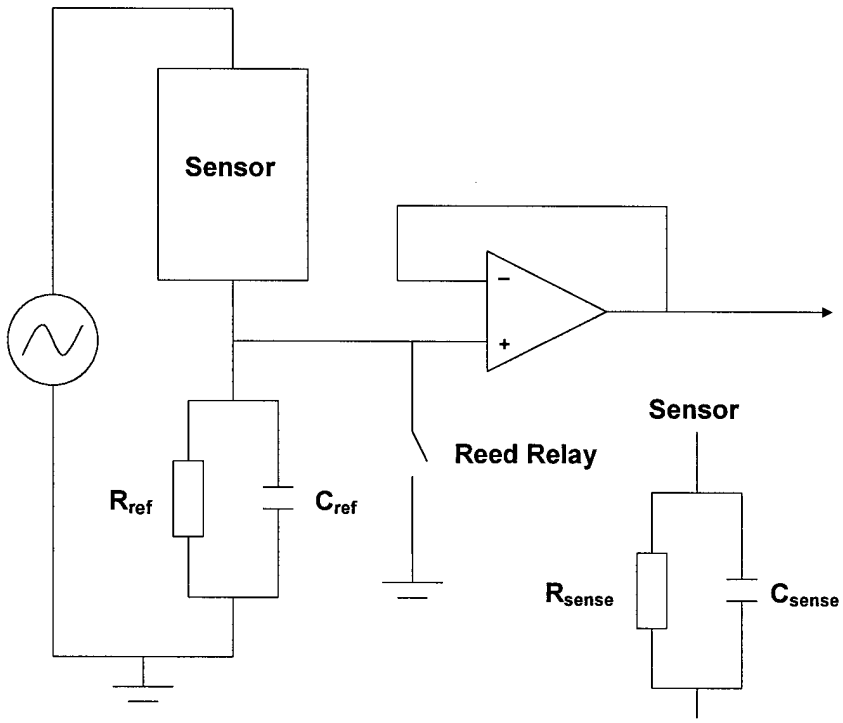

Figure 7. Circuit schematic for a single channel.

Software was written in LabView to acquire a complex voltage signal from each channel on the circuit and reduce this signal to its gain and phase components. The conductance and capacitance can be inferred from (7) and (8), respectively, where V is the gain, θ is the phase, ω is the angular frequency, C_r is the reference capacitance, and G_r is the reference conductance.

$$G_{sense} = -\frac{V \cdot (\sin(\theta) \cdot \omega \cdot C_r - \cos(\theta) \cdot G_r + V \cdot G_r)}{V^2 - 2 \cdot V \cdot \cos(\theta) + 1} \tag{7}$$

$$C_{sense} = -\frac{V \cdot (-\omega \cdot C_r \cdot \cos(\theta) + \omega \cdot V \cdot C_r - \sin(\theta) \cdot G_r)}{\omega \cdot (V^2 - 2 \cdot V \cdot \cos(\theta) + 1)} \tag{8}$$

RESULTS AND DISCUSSION

This section first discusses numerical results for predicted fill front position and compares these results to the experimentally observed fill front position. Developing analytical equations that can accurately predict the fill front position is an important step in being able to implement adaptive control in RTM. Numerical simulations of the sensor will then be discussed, followed by the experimental results obtained with the RTM setup using water/glycerin filler and by results obtained with the VARTM setup using polymer resins.

Predicted Fill-Front Position

The average fluid velocity $\bar{V}$ through the porous preform is

$$\bar{V} = \frac{Q_{mold}}{A_{frac}} \tag{9}$$

where Q_{mold} is the volumetric flow rate in the mold and A_{frac} is the cross-sectional area of the mold perpendicular to the direction of the flow and not occupied by the porous medium. From Darcy's law, the flow from the leading edge of the porous medium to the fill front is described by

$$\bar{V} = -\frac{k}{\mu}\frac{\partial P}{\partial x} \tag{10}$$

where $\bar{V}$ is the average velocity of the fluid, k is the permeability of the porous medium, μ is the viscosity of the fluid and $\frac{\partial P}{\partial x}$ is the pressure gradient in the x direction. The pressure change for a one-dimensional flow through an isotropic porous medium is linear. Therefore the average velocity can be written as

$$\bar{V} = \frac{k}{\mu}\frac{P_{in} - P_{fillfront}}{x} \tag{11}$$

where x is the distance from the leading edge of the porous medium to the fill front and P_{in} is a function of x. Expressing the pressures as gauge pressures, (9) and (11) can be combined to give

$$\bar{V} = \frac{dx}{dt} = \frac{k}{\mu}\frac{P_{in}}{x} \tag{12}$$

since $P_{fillfront}$ is atmospheric pressure. A complete derivation of P_{in} is given in [39]. The result is stated here:

$$P_{in} = \frac{A + B \pm \sqrt{(A+B)^2 - 32CD^4\left[P_{res} - \rho g\left(h_0 + \frac{A_{fr}}{A_{re}}x\right)\right]}}{\frac{16C}{\pi}} \tag{13}$$

where

$$A = 128 l_{eq} \frac{kA_{fr}}{x} \tag{14}$$

$$B = \pi D^4 \tag{15}$$

$$C = \rho\left(\frac{kA_{fr}}{\mu x}\right)^2 \tag{16}$$

x is the flow front location, P_{in} is the inlet pressure recorded, l_{eq} is the equivalent length of tubing, k is the permeability of porous medium, A_{fr} is the cross sectional area of the mold perpendicular to the direction of the fluid flow not occupied by the porous material, A_{re} is the cross sectional area of the reservoir, μ is the viscosity of the fluid, D is the inside diameter of the tube, P_{res} is the pressure in the pressure pot, h_0 is the initial height difference between the fluid level in pot and the inlet port when the fill front is at the leading edge of porous medium and ρ is the density of the fluid. The values used in the numerical simulation are l_{eq} = 0.66 m, A_{fr} = 0.00309 m^2, D = 0.00432 m, ρ = 1220 kg/m^3, h_0 = 0.4 m ,A_{re} = 0.0415 m^2, μ = 0.089 Ns/m^2, and k = 2.51x10^{-9} m^2. The viscosity and density values of the water/glycerin solution were taken from the manufacturer's specification sheet.

Equation 12 can be rearranged as follows to give the fill front position as a function of time

$$\int_0^t \frac{k}{\mu} dt = \int_0^x \frac{x'}{P_{in}} dx' \tag{17}$$

$$\frac{k}{\mu} t = \int_0^x \frac{x'}{P_{in}} dx' \tag{18}$$

The above equation expresses the fill front position at any time as a function of the reservoir pressure alone. It is numerically solved for x after substituting for P_{in} from (13).

Figure 8 shows comparisons between experimental data obtained visually and predicted data for varying reservoir pressures. As the pressure was increased, a corresponding fall in the fill time was observed. It was also noted that there was a slight deviation of predicted values from the experimental results, which is attributed mostly to a rounding error in the inlet pressure readings.

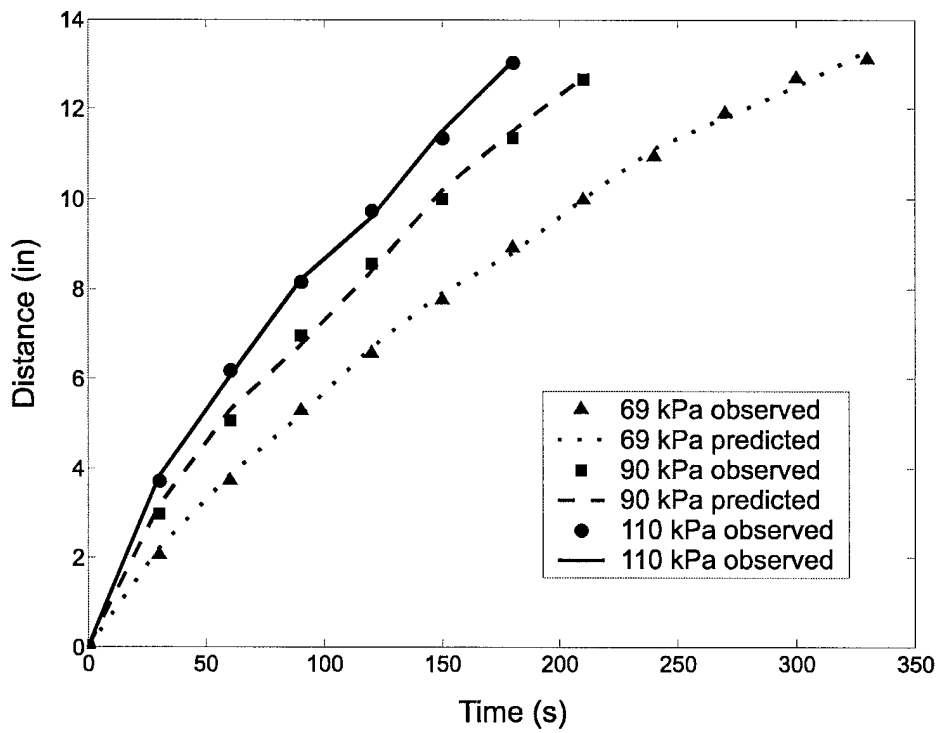

Figure 8. Comparison between experimental (visual) and predicted data for varying reservoir pressures (69, 90, 110 kPa).

The good agreement between visually recorded flow front position and theoretically predicted position suggests that the system is sufficient for simulating industrial resin transfer molding processes. It follows that a sensor technique capable of monitoring flow front position on this system will also measure position accurately on an industrial setup.

Predicted Sensor Performance

The numerical simulations were performed with Maxwell software by Ansoft Corp. Each transparent sensor was modeled as a cross-section of infinite depth on a per-meter length basis. A parametric simulation of each sensor was run in order to find the predicted capacitance as a function of flow-position along the mold. Figure 9 shows the distribution of equipotential lines and electric field in and around the dielectric cell. Figure 9 also shows the uniformity of the field between the sensing and driving electrodes, whereas the field begins to fringe between the guard and drive electrodes. Figure 10 shows the results of the numerical simulation for a single sensor.

The numerical simulations are used to produce an accurate transfer function between the measured capacitance and conductance values and the position of the fill front inside the mold. In the absence of fringing field effects, the sensors would record fill front progression only when the liquid is directly between the sensing and driven electrodes of the parallel-plate setup. Since the exact position of the sensors on the mold is known *a priori*, a measurable change in sensor signal directly corresponds to position of the fill front. Fringing field effects, however, cause the sensor to measure fill front progression before the liquid is directly underneath the sensor, thus preventing a direct calculation of the fill front position from the measured capacitance and conductance. These effects can be seen in the early and late stages of the numerical data shown in Figure 10.

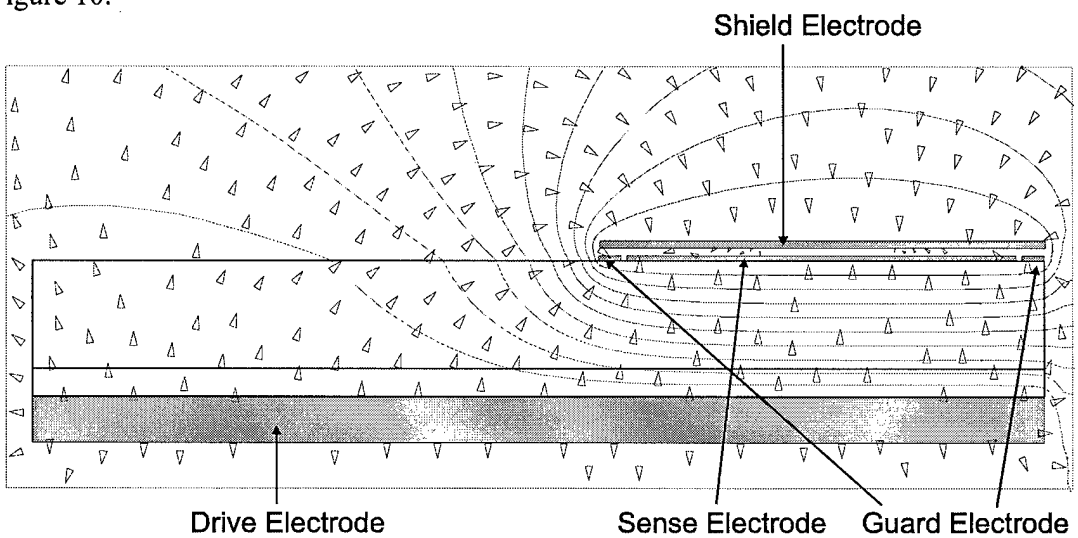

Figure 9. Equipotential lines and distribution of the electric field in and around the dielectric cell. The size of the arrows is logarithmically proportional to the intensity of the electric field.

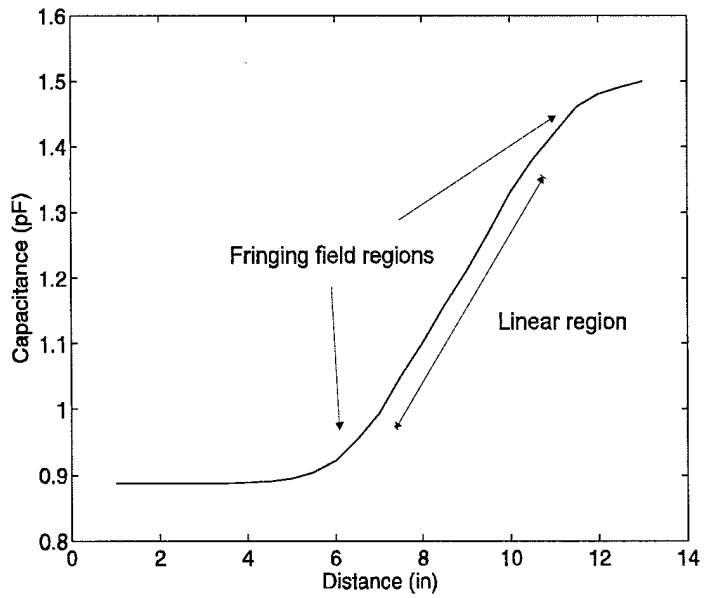

Figure 10. Numerical results for a single sensor. The geometry and position of the sensor on the mold determines the characteristic curve.

It is important to compare the numerical results to theoretically predicted values for a guarded parallel plate capacitor in order to ensure the accuracy of the simulation. The analytical expression for the capacitance of the heterogeneous material inside the mold can be calculated using a lumped circuit approximation of the layered medium. The capacitance contributed by the dielectric permittivity of the Lexan plate and air can be represented by a series combination of capacitors. When the mold fills, the air is replaced with water/glycerin solution and the capacitor previously representing the air now represents the water/glycerin solution. The analytical expression for the capacitance is

$$C = \varepsilon_0 \cdot A \cdot \left[\frac{1}{\left(\frac{d_1}{\varepsilon_1}\right) + \left(\frac{d_2}{\varepsilon_2}\right)} \right] \tag{19}$$

where A is the area of the sensing electrode, d_1 is the thickness of the Lexan plate, d_2 is the air gap thickness, and ε_1 and ε_2 are the dielectric permittivities of Lexan and air, respectively. For this study $\varepsilon_1 \approx 3.1$ and $\varepsilon_2 \approx 1$. The presence of pre-form typically increases ε_2 by a factor of 1.1 to 1.5. The analytical expression gives an empty-mold capacitance of 0.8257 pF, while the numerical simulations predict a value of 0.887 pF. The close agreement of these two values suggests that the numerical simulations take into account the secondary edge effects described previously. The material properties of the water/glycerin solution were measured using a simple dielectric cell and are in good agreement with values taken from the data sheet provided by the manufacturer. The dielectric constant of the solution was $\varepsilon_{2*} \approx 46$. This value was used in the analytical expression as well as the Maxwell simulations. When the mold is filled with

water/glycerin solution, the analytical capacitance is 1.532 pF, while numerical simulations predict a value of 1.500 pF.

Experimental Capacitance and Phase Data

Terminal admittance values were acquired using the dielectric sensor array system. Gain and phase were measured by the sensors and converted to capacitance and conductance values. Cross-talk between parallel plate sensors was observed during experiments. The effect of the cross-talk on the measured capacitance was negligible considering that measured capacitance values from one sensor, driven alone and driven simultaneously with two other sensors, differed by less than 1 percent.

Figure 11 shows experimental results for an experiment at 90 kPa. The data exhibits a gradual increase in capacitance as the fluid flows through the mold. This gradual increase is predicted by numerical simulations and is due to edge effects of the parallel-plate setup. The water/glycerin solution is detected by the sensors before the liquid is actually between the plates. Numerical simulations can quantify this effect so that it can be factored out.

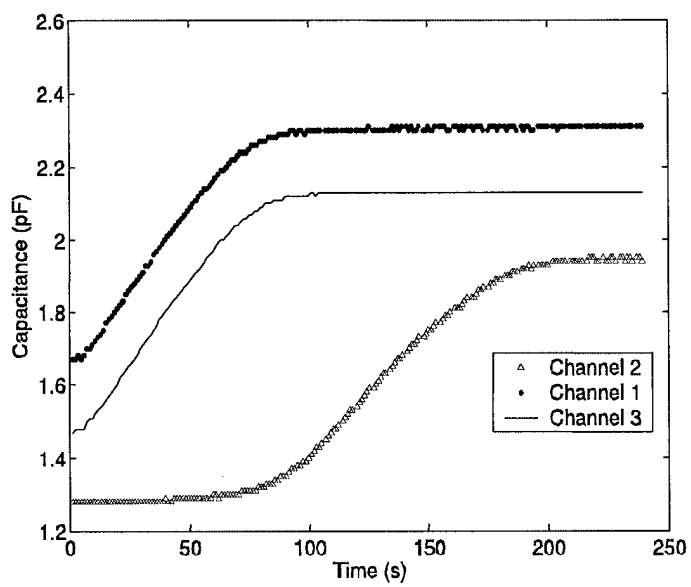

Figure 11. Capacitance as a function of time for three sensors at 90 kPa.

The signal to noise ratio (SNR) for the capacitance data is found by taking the magnitude of the signal and dividing by the magnitude of the observed noise in the data set. Using channel 1 from Figure 11 as an example, the SNR is given by

$$SNR_{cap} = \frac{signal}{noise} = \frac{(2.31-1.67)}{0.01} = 64 \tag{20}$$

Converting to decibels yields an SNR of 18 dB. The uncertainty in the flow front measurement can be found since the SNR of the flow front measurement will be the same. The uncertainty calculation in the flow measurement is given by

$$noise_{flow} = \frac{signal}{SNR_{cap}} = \frac{(6.5)}{64} = 0.101 \tag{21}$$

thus, the uncertainty in the flow measurement is +/- 0.101 inches or +/- 2.57 mm.

Data Analysis

A mapping algorithm was developed to convert measured capacitance values to flow front position as a function of time for each sensor. Figure 12 shows a graphical representation of this algorithm.

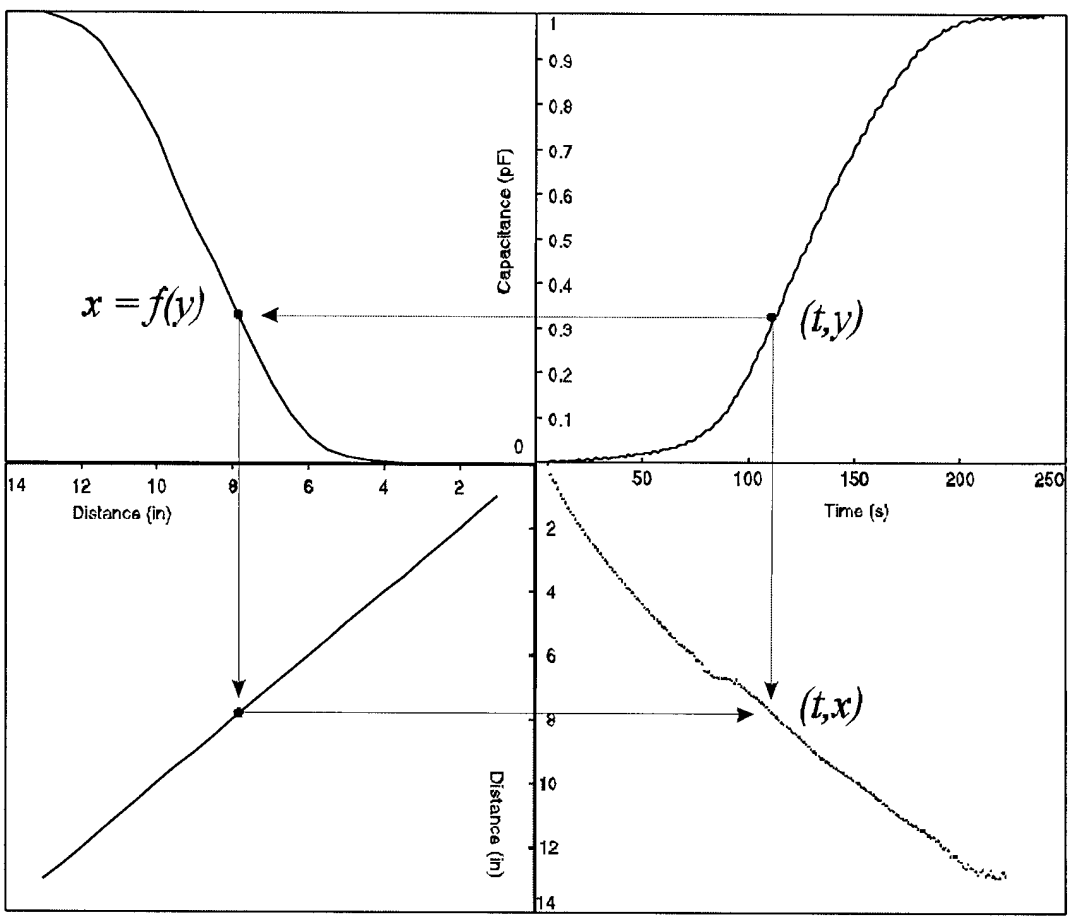

Figure 12. Graphical representation of the mapping algorithm used in the data analysis.

The algorithm includes a normalization procedure and curve fitting routine detailed below:

(1) Normalize experimental and numerical data. For this normalization procedure, assume only errors of the form $ax+b$. Zero the data by subtracting the lowest value ('b') from each data point. Then divide each new data point by the highest value data point, eliminating 'a'. This step is implemented in quadrants 1 and 2 of Figure 12.
(2) Use a spline curve-fitting method to fit a curve to the normalized numerical data. A spline fit will draw curves between consecutive data points and will find the equation for each curve. Thus, there is an equation describing any region on the graph containing two consecutive points, instead of one equation describing the region encapsulated by all points. This step is implemented in quadrant 2.
(3) Substitute in each experimental capacitance value (with its corresponding time) to this equation and find the distance at which this capacitance was measured. This step is implemented in quadrant 3.
(4) Plot distance as a function of time for each sensor. This step is implemented in quadrant 4.

This method is used because it can easily be developed into a fast real-time algorithm once the respective look-up tables are generated for each sensor. For example, if the sensor geometry and relative position on the mold is kept constant, only one numerical simulation is needed to correlate a measured capacitance with a distance along the mold. The graphical representation allows the reader to visualize the steps described above. The first and second quadrants of Figure 12 correspond to steps 1 and 2 of the algorithm above. Quadrant 3 corresponds to step 3 of the algorithm and quadrant 4 corresponds to step 4 of the algorithm. It should be noted that when the sensor geometry or position on the mold changes, additional numerical simulations will be needed in order to develop a mapping routine.

Flow-Front Position

Figure 13 shows that the fill front measurement by the sensor system is in good agreement with the positions recorded by the video camera. The maximum difference between the visual and experimental data is approximately 0.2 inches (5 mm). The measurement accuracy is lowest in the region between the two sensors. This larger error in the region between the sensors is observed because the measurements are inherently less accurate due to fringing field effects.

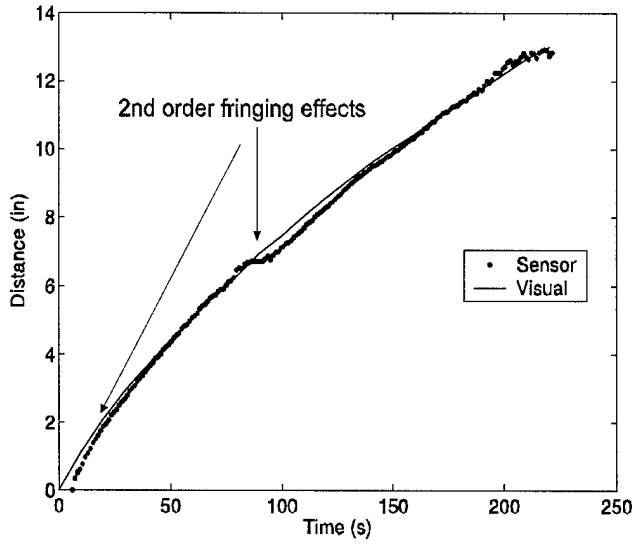

Figure 13. Visual and experimental comparison of measured fill-front position at the centerline at 90 kPa.

Although dielectric properties of resins are different from dielectric properties of glycerin-water mixtures, measurement of fill front position works equally well, because sensor response is strong in both cases.

Figure 14 shows the visual and sensor data for fill front position in a VARTM process using STYPOL 040-3676, a general purpose polyester resin. For this experiment, fringing field sensors, which require only one-sided access to the mold, were used. A good agreement between visual and sensor flow-front is observed.

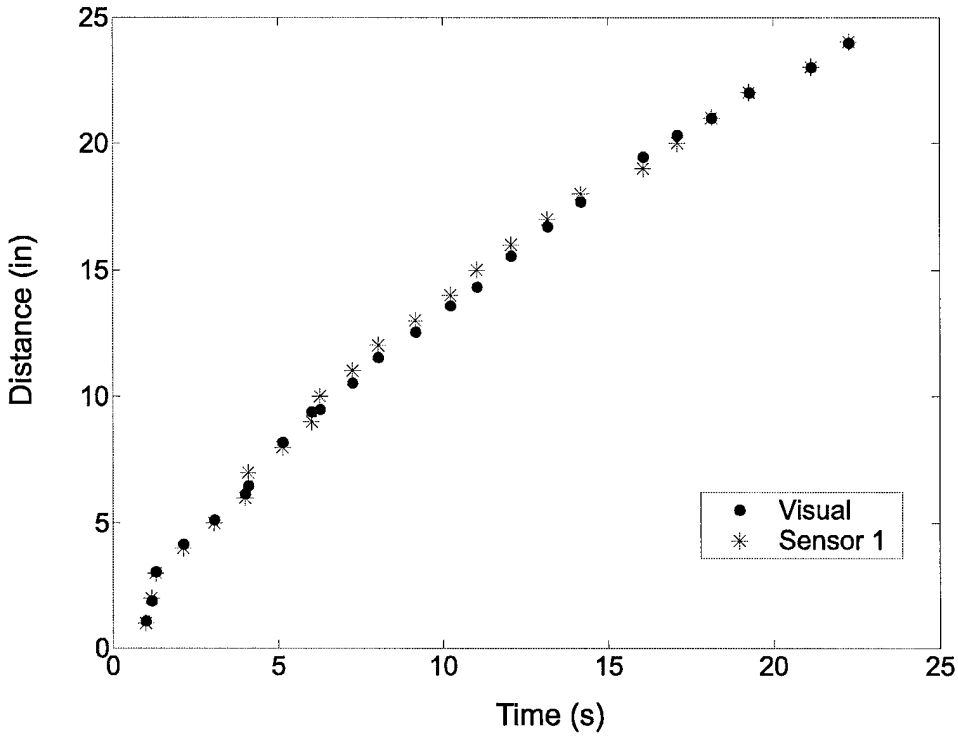

Figure 14. Visual and experimental comparison of measured fill-front position at the centerline at 90 kPa for VARTM process using resin.

After the filling process is complete, the sensor array switches into cure mode by measuring the curing process of the resin. An extended analysis of cure monitoring is the subject of a subsequent publication. As an illustration of dielectric spectroscopy signature, Figure 15 shows electrical parameter measurements as a function of frequency for the resin during the curing phase.

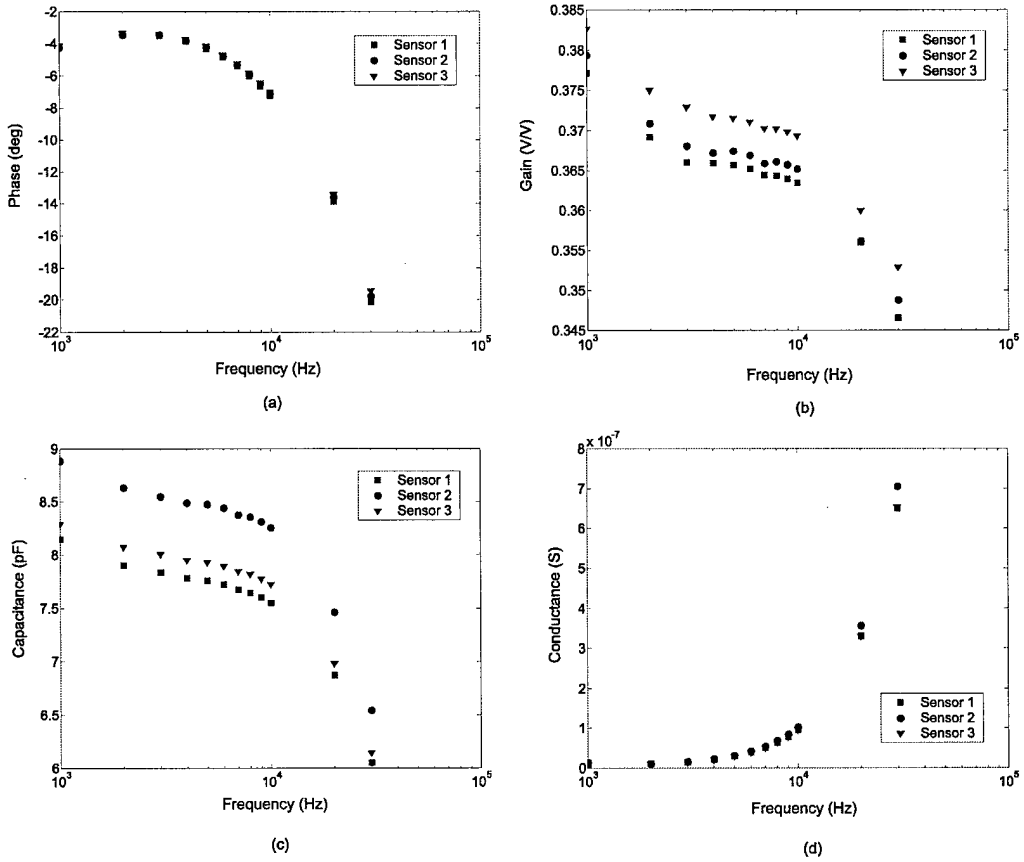

Figure 15. Electrical parameter measurements of the resin during cure, as a function of frequency: (a) phase (b) gain (c) capacitance (d) conductance

Gain and capacitance show a similar monotonic decrease with frequency across all three channels, while phase and conductance monotonically increases with frequency. These spectroscopy measurements can be used as part of a calibration-based sensing technique to characterize the curing cycle of the resin.

CONCLUSIONS

A distributed dielectric sensor array for measurement of flow front location in RTM and VARTM processes was designed and tested with water/glycerin mixtures and with industrial resins. These sensors are also capable of monitoring degree of cure of resin. The developed technique allows for continuous sensing over the entire mold while being completely non-invasive and not requiring embedded materials. The technique is useful for manufacturing of composite materials, where adaptive feed-forward control of the manufacturing process is desired. In addition, the sensor arrays can be made completely transparent, allowing for good visual calibration and the possibility of a coupled infrared sensor system.

Further details on this research can be found in the cited publications resulting from this project in section 3 of this report.

REFERENCES

[1] K. Han and L. J. Lee, "Dry Spot Formation and Changes in Liquid Composites Molding: I-Experiments," *Journal of Composite Materials*, vol. 30, pp. 1458-1474, 1996.

[2] K. Han, L. J. Lee, and S. Nakamura, "Dry Spot Formation and Changes in Liquid Composites Molding: II-Modeling and Simulation," *Journal of Composite Materials*, vol. 30, pp. 1475-1493, 1996.

[3] J. Mogavero, J. Q. Sun, and S. G. Advani, "A Nonlinear Control Method for Resin Transfer Molding," *Polymer Composites*, vol. 18, no. 3, pp. 412-417, June 1997.

[4] M. K. Yoon and J. Q. Sun, "Adaptive Control of Flow Progression in Resin Transfer Molding," *Journal of Materials Processing & Manufacturing Science*, vol. 10, no. 3, pp. 171-182, Jan. 2002.

[5] D. D. Shepard, "Resin Flow Front Monitoring Saves Money and Improves Quality," *SAMPE Journal*, vol. 34, no. 6, pp. 31-35, Nov. 1998.

[6] B. Berker, P. Barooah, and J. Q. Sun, "Sequential Logic Control of Liquid Injection Molding With Automatic Vents and Vent-to-Gate Converters," *Journal of Materials Processing & Manufacturing Science*, vol. 6, no. 2, pp. 81-103, Oct. 1997.

[7] H. H. Demirci and J. P. Coulter, "A Comparative Study of Nonlinear Optimization and Taguchi Methods Applied to the Intelligent Control of Manufacturing Processes," *Journal of Intelligent Manufacturing*, vol. 7, no. 1, pp. 23-38, Feb. 1996.

[8] S. Parthasarathy, S. C. Mantell, K. A. Stelson, S. Bickerton, and S. G. Advani, "Real-Time Sensing and Control of Resin Flow in Liquid Injection Molding Processes," *Proceedings of the 1998 American Control Conference*, vol. 4, pp. 2181-2184, 1998.

[9] S. H. Ahn, W. I. Lee, and G. S. Springer, "Measurement of the 3-Dimensional Permeability of Fiber Preforms Using Embedded Fiber Optic Sensors," *Journal of Composite Materials*, vol. 29, no. 6, pp. 714-733, 1995.

[10] J. R. Bernstein and J. W. Wagner, "Fiber Optic Sensors for Use in Monitoring Flow Front in Vacuum Resin Transfer Molding Processes," *Review of Scientific Instruments*, vol. 68, no. 5, pp. 2156-2157, May 1997.

[11] Crosby, P. A., Powell, G. R., Fernando, G. F., Waters, D. N., France, C. M., and Spooncer, R. C., "*A Comparative Study of Optical Fibre Cure Monitoring Methods*", SPIE, 1997, pp. 141-153.

[12] D. D. Shepard and K. R. Smith, "Ultrasonic Cure Monitoring of Advanced Composites," *Sensor Review*, vol. 19, no. 3, pp. 187-191, 1999.

[13] P. A. Fomitchov, Y. K. Kim, A. K. Kromine, and S. Krishnaswamy, "Laser Ultrasonic Array System for Real-Time Cure Monitoring of Polymer-Matrix Composites," *Journal of Composite Materials*, vol. 36, no. 15, pp. 1889-1901, 2002.

[14] D. L. Woerdeman and R. S. Parnas, "Cure Monitoring in Rtm Using Fluorescence," *Plastics Engineering*, vol. 51, no. 10, pp. 25-&, Oct. 1995.

[15] S. M. Tavakoli, M. Avella, and M. G. Phillips, "Fiber Resin Compatibility in Glass Phenolic Laminating Systems," *Composites Science and Technology*, vol. 39, no. 2, pp. 127-145, 1990.

[16] P. Barooah, B. Berker, and J. Q. Sun, "Lineal Sensors for Liquid Injection Molding of Advanced Composite Materials," *Journal of Materials Processing & Manufacturing Science*, vol. 6, no. 3, pp. 169-184, Jan. 1998.

[17] C. W. Lee, B. P. Rice, M. Buczek, and D. Mason, "Resin Transfer Process Monitoring and Control," *SAMPE Journal*, vol. 34, no. 6, pp. 48-55, Nov. 1998.

[18] S. D. Schwab, R. L. Levy, and G. G. Glover, "Sensor System for Monitoring Impregnation and Cure During Resin Transfer Molding," *Polymer Composites*, vol. 17, no. 2, pp. 312-316, Apr. 1996.

[19] I. Alig, W. Jenninger, M. Junker, and L. A. deGraaf, "Dielectric Relaxation Spectroscopy During Isothermal Curing of Semi-Interpenetrating Polymer Networks," *Journal of Macromolecular Science-Physics*, vol. B35, no. 3-4, pp. 563-577, 1996.

[20] A. A. Potapov, "Temperature-Dielectric Spectroscopy of Solutions," *Instruments and Experimental Techniques*, vol. 36, no. 5, pp. 772-776, Sept. 1993.

[21] D. Kranbuehl, D. Hood, A. Kriss, R. Barksdale, A. C. Loos, J. D. Macrae, and G. Hasko, "Insitu FDEMS Sensing and Modeling of Epoxy Infiltration, Viscosity and Degree of Cure During Resin Transfer Molding of a Textile Preform," *Abstracts of Papers of the American Chemical Society*, vol. 211, pp. 17-MSE, Mar. 1996.

[22] D. Kranbuehl, M. Hoff, D. Eichinger, R. Clark, and A. Loos, "Monitoring and Modeling the Cure Processing Properties of Resin Transfer Molding Resins," *International SAMPE Symposium and Exhibition*, vol. 34, 1989, pp. 416-425.

[23] D. E. Kranbuehl, P. Kingsley, S. Hart, G. Hasko, B. Dexter, and A. C. Loos, "In-Situ Sensor Monitoring and Intelligent Control of the Resin Transfer Molding Process," *Polymer Composites*, vol. 15, no. 4, pp. 299-305, Aug. 1994.

[24] D. Kranbuehl, S. Delos, M. Hoff, L. Weller, P. Haverty, and J. Seeley, "Frequency-Dependent Dielectric Analysis - Monitoring the Chemistry and Rheology of Thermosets During Cure," *ACS Symposium Series*, vol. 367, pp. 100-112, 1988.

[25] M. Rooney, P. J. Biermann, B. G. Carkhuff, D. R. Shires, and R. V. Mohan, "Development of In-Process RTM Sensors for Thick Composite Sections," *Proceedings of the 1998 American Control Conference*, vol. 6, 1998, pp. 3875-3878.

[26] A. A. Skordos, P. I. Karkanas, and I. K. Partridge, "A Dielectric Sensor for Measuring Flow in Resin Transfer Moulding," *Measurement Science & Technology*, vol. 11, no. 1, pp. 25-31, Jan. 2000.

[27] A. von Hippel, *Dielectric Materials and Applications,* Artech House, 1995.

[28] I. G. Matis, "Method And Equipment For Determining The Dielectric Constant Of Polymer Materials With One-Sided Access," *Polymer Mechanics*, vol. 2, no. 4, pp. 380-383, 1966.

[29] S. D. Senturia, N. F. Sheppard, S. Y. Poh, and H. R. Appelman, "The Feasibility of Electrical Monitoring of Resin Cure With the Charge-Flow Transistor," *Polymer Engineering and Science*, vol. 21, no. 2, pp. 113-118, Feb. 1981.

[30] S. D. Senturia, N. F. Sheppard Jr, H. L. Lee, and D. R. Day, "In-Situ Measurement of the Properties of Curing Systems With Microdielectrometry," *Journal of Adhesion*, vol. 15, no. 69, pp. 69-90, 1982.

[31] S. D. Senturia and S. L. Garverick, "Method and Apparatus for Microdielectrometry," US Patent No.4,423,371, Dec. 1983.

[32] M. C. Zaretsky, L. Mouayad, and J. R. Melcher, "Continuum Properties From Interdigital Electrode Dielectrometry," *IEEE Transactions on Electrical Insulation*, vol. 23, no. 6, pp. 897-917, Dec. 1988.

[33] A. Washabaugh, D. E. Schlicker, A. V. Mamishev, M. Zahn, and N. Goldfine, "Dielectric Sensor Arrays for Monitoring of Aging in Composites and Other Low-Conductivity Media," *SPIE Conference*, 1999,

[34] J. Mijovic and J. W. Sy, "Dipole Dynamics and Macroscopic Alignment in Molecular and Polymeric Liquid Crystals by Broad-Band Dielectric Relaxation Spectroscopy," *Macromolecules*, vol. 33, no. 26, pp. 9620-9629, Dec. 2000.

[35] D. E. Kranbuehl, S. E. Delos, and E. Yi, "Measurement and Application of Dielectric Properties," *SPIE Technical Papers*, vol. 31, no. 311, pp. 73-90, 1985.

[36] A. V. Mamishev, Y. Du, B. C. Lesieutre, and M. Zahn, "Development and Applications of Fringing Electric Field Dielectrometry Sensors and Parameter Estimation Algorithms," *Journal of Electrostatics*, vol. 46, no. 2-3, pp. 109-123, Apr. 1999.

[37] N. J. Goldfine, "Magnetometers for Improved Materials Characterization in Aerospace Applications," *Materials Evaluation*, vol. 51, no. 3, pp. 396-405, Mar. 1993.

[38] A. V. Mamishev, B. C. Lesieutre, and M. Zahn, "Optimization of Multi-Wavelength Interdigital Dielectrometry Instrumentation and Algorithms," *IEEE Transactions on Dielectrics and Electrical Insulation*, pp. 408-420, 1998.

[39] C. B. Ebersold, "*Racetracking and Porous Medium Displacement in Resin Transfer Molding*,", Department of Mechanical Engineering, University of Washington, 2000.

SECTION 3: LIST OF PUBLICATIONS RESULTING FROM THIS PROJECT

To date, the work related to this project has been published in four journal papers, ten conference papers, and two master theses. Further details on this research can be found in the cited publications resulting from this project that are listed below.

Journal Papers

1. B. Minaie, Y.F. Chen, and A.M. Mescher, "A Methodology To Obtain A Desired Filling Pattern During Resin Transfer Molding," Journal of Composite Materials, Vol. 36, No. 14, pp. 1677-1692, 2003.
2. B. Minaie and Y.F. Chen, "Adaptive Control of Filling Pattern in Resin Transfer Molding Process," Journal of Composite Materials (accepted).
3. A.V. Mamishev, K. Sundara-Rajan, F. Yang, Y. Du, M. Zahn, "Interdigital Sensors and Transducers," Proceedings of the IEEE, vol. 92, no. 5, 2004, pp. 808-845 (invited paper).
4. M. Hegg, A. Ogale, A. Mescher, A.V. Mamishev, B. Minaie, "Remote Monitoring of Resin Transfer Molding Processes by Distributed Dielectric Sensors," Journal of Composite Materials (accepted).

Conference Papers

1. B. Minaie, S. Jiang, W. Li, K.T. Hsiao, and R. Little, "Adaptive Control of Non-Isothermal Resin Transfer Molding Process," 49th International SAMPE Symposium, 2004.
2. R. Panitapu, S. Jiang, and B. Minaie, "Time-Implicit Simulation of Filling Pattern in Resin Transfer Molding Using Control Volume Finite Difference Method," 49th International SAMPE Symposium, 2004.
3. B. Minaie, W. Li., J. Gou, Y. Chen, A. Mamishev, and A. Mescher, "Direct Adaptive Control of Resin Transfer Molding," 48th International SAMPE Symposium Proceedings, pp. 646-657, May 11-15, 2003.
4. C. Myint, K.T. Hsiao, B. Minaie, "Review of Manufacturing Functionally Graded Materials," ASME Annual Journal for Region XI RTC, 2004.
5. O. Restrepo, K.T. Hsiao, S. Jiang, B. Minaie , "Preliminary Study and Implementation of Adaptive Control for Resin Transfer Molding," ASME Annual Journal for Region XI RTC, 2004.
6. R.K. Panitapu, S. Jiang, B. Minaie, "Analysis of Filling Pattern in Resin Transfer Molding," ASME Annual Journal for Region XI RTC, 2004.
7. Ogale, M. Hegg, A. Mescher, A. V. Mamishev, and B. Minaie, "Fill Front Detection Using Dielectric Sensors In Resin Transfer Molding Process," ICCE, New Orleans, LA, 2003.
8. M.C. Hegg, M. J. Kim, A.V. Mamishev, "Influence of Variable Plate Separation on Fringing Electric Fields in Parallel-Plate Capacitors," IEEE ESEI Conference, Indiana, 2004, pp. 384-387.

9. X. B. Li, S. D. Larson, A. S. Zyuzin, and A. V. Mamishev, " Design of Multi-channel Fringing Electric Field Sensors for Imaging – Part I: General Design Principles," IEEE ESEI Conference, Indiana, 2004, pp. 406-409.
10. X. B. Li, C. Kato, A. S. Zyuzin, and A. V. Mamishev, " Design of Multi-channel Fringing Electric Field Sensors for Imaging – Part II: Numerical Examples," IEEE ESEI Conference, Indiana, 2004, pp. 410-413.

Theses

1. Ravi Panitapu, "Analysis of Filling Pattern in Resin Transfer Molding," Master Thesis, Department Of Mechanical Engineering, University Of South Alabama, 2003.
2. Michael C. Hegg, "Monitoring of Resin Transfer Molding Processes with Distributed Dielectric Sensors," Master Thesis, Department of Electrical Engineering, University of Washington, 2004.